Single diffractive production of open heavy flavor mesons

Marat Siddikov and Iván Schmidt

Departamento de Física, Universidad Técnica Federico Santa María, y Centro Científico—Tecnológico de Valparaíso, Casilla 110-V, Valparaíso, Chile

(Received 2 September 2020; accepted 6 October 2020; published 28 October 2020)

In this paper, we discuss the single diffractive production of open heavy flavor mesons and nonprompt charmonia in pp collisions. Using the color dipole approach, we found that the single diffractive production constitutes 0.5%–2% of the inclusive production of the same mesons. In Tevatron kinematics, our theoretical results are in reasonable agreement with the available experimental data. In LHC kinematics, we found that the cross section is sufficiently large and could be accessed experimentally. We also analyzed the dependence on multiplicity of coproduced hadrons and found that it is significantly slower than that of inclusive production of the same heavy mesons.

DOI: 10.1103/PhysRevD.102.076020

I. INTRODUCTION

In the kinematics of the LHC, the diffractive events in pp collisions constitute approximately 20% of all inclusive events [1] and for this reason might be used as an additional tool for studies of the strong interactions. The characteristic feature of the diffractive events is the presence of rapidity gaps between hadronic products in the final state. In QCD, such rapidity gaps in high-energy kinematics are explained by the exchange of Pomerons in the t-channel. Since the structure of the Pomeron is relatively well understood and largely does not depend on the process, the existence of the rapidity gap allows us to separate the strong interactions involving different hadrons. While conventionally diffractive production of mesons has been studied in ep collisions, there are various theoretical suggestions to use pp collisions for studies of the diffractive production of prompt quarkonia [2–6], dijets [7], gauge bosons [8], Higgs bosons [9], heavy quarks [10–12], quarkonia pairs [13], and Drell-Yan processes [14]. The possibility of measuring diffractive production in pp collisions has been demonstrated at the Tevatron [15–19], while at the LHC, some diffractive processes (e.g., single diffractive $pp \to pX$) have been measured with very good precision [1], although diffractive production of additional heavy hadrons so far has not been explored in depth (see, however, the preliminary feasibility study [20]).

In this paper, we are going to focus on single diffractive production of heavy mesons, $pp \to p + MX$, where M is an open heavy flavor meson (D or B) or a charmonium produced from decay of B meson; we also assume that the recoil proton in the final state is separated by a rapidity gap from other hadrons. This process deserves special interest both on its own and because it could help to clarify the role of multi-Pomeron contributions to the production of heavy quarks in general. The role of such mechanisms is not very clear at this moment. Usually, it is believed that production of heavy quarks might be described perturbatively [21,22] and is dominated by two-gluon (Pomeron) fusion [23–31]. However, this approach can hardly explain the recently measured dependence of the production cross sections on the multiplicity of the charged hadrons coproduced together with a given heavy quarkonia [32–37]. Potentially, this discrepancy might indicate sizeable contributions of multigluon production mechanisms. At the same time, for D and B mesons, such rapidly growing dependence was not observed [32]. On the other hand, theoretical studies [38–40] found that three-Pomeron mechanism might give sizeable contribution and can explain the observed multiplicity dependence of quarkonia, while for D mesons, it was found in the same framework that the three-Pomeron correction is also pronounced and might constitute up to 40% of the result, although in the range of multiplicities available at present from the LHC, it does not contribute to the observed multiplicity dependence due to partial cancellation with certain interference contributions [41]. Fortunately, it is possible to estimate the role of the three-Pomeron fusion directly. The single diffractive production at the partonic level has a similar structure and thus might provide an independent estimate of the three-Pomeron contribution. Since the single diffractive production amplitude includes only one cut Pomeron which might contribute to the observed yields of coproduced hadrons, its cross section might be used as a very

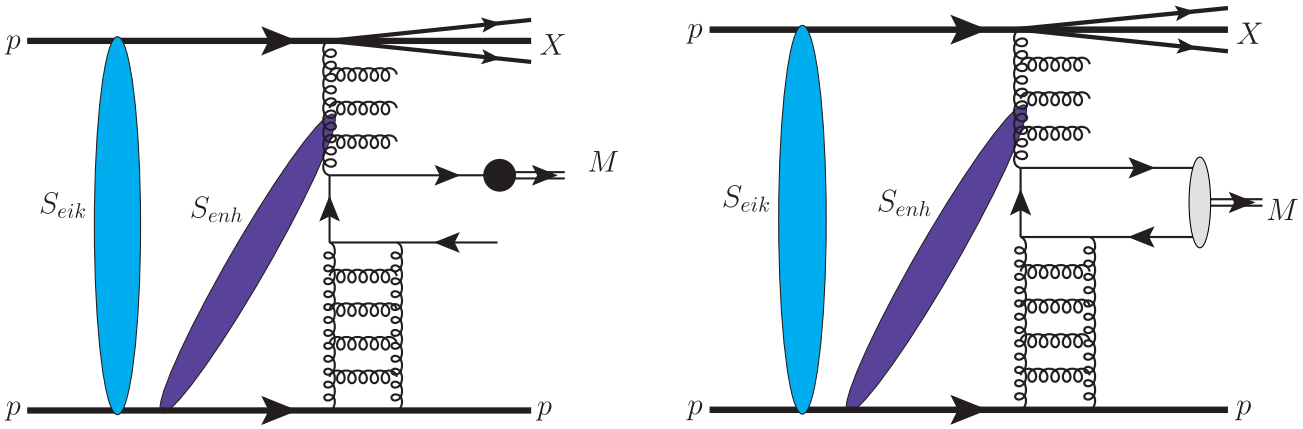

FIG. 1. Left plot: the leading-order contribution to single diffractive production of open heavy flavor quark mesons. The recoil proton (lower part) is separated from the heavy hadron by a rapidity gap. The colored vertical and inclined ovals schematically illustrate the contributions of the secondary interactions, whose products might fill the rapidity gap between the recoil proton and the other hadrons (see the text for discussion). Right plot: the leading-order contribution to the single diffractive production of prompt charmonia studied in Refs. [4–6].

clean probe of the multiplicity dependence of individual cut Pomerons in high-multiplicity events.

Earlier, the single diffractive production including heavy quarks was studied in Refs. [10–12] for the case of prompt production of quarkonia. As we will see below, the cross sections of single diffractive production of D and B mesons is larger than that of the prompt charmonia and thus could be easier to study experimentally. The feasibility to measure such processes has been discussed in Refs. [15,16,20], although the study of rare events with large multiplicity requires better statistics, and for this reason, we expect that such dependence could be measured during the High Luminosity Run 3 at the LHC [42–44].

The paper is structured as follows. In Sec. II, we develop the general framework for the evaluation of the open heavy meson production. We will perform our calculations within the color dipole framework, which describes correctly the onset of saturation dynamics and thus might be used even for the description of high multiplicity events. In Sec. III, we present our numerical results and make comparison with experimental data available from the Tevatron, as well as with other theoretical approaches. In Sec. IV, we develop the framework for the description of multiplicity dependence in the dipole framework and compare its predictions for multiplicity dependence with that of inclusive production. In Sec. V, we discuss briefly the single diffractive process on nuclei, $pA \to p + MX$. Finally, in Sec. VI, we draw conclusions.

II. SINGLE-DIFFRACTIVE PRODUCTION IN COLOR DIPOLE FRAMEWORK

As was mentioned in the previous section, a defining characteristics of the single diffractive production is the observation of the recoil proton separated by a large rapidity gap from other hadrons. In LHC kinematics, the dominant contribution to such a process stems from the diagrams which include the exchange of an uncut Pomeron between the proton and the other hadrons in the t-channel. The heavy mesons are produced predominantly near the edge of the rapidity gap, and for this reason, a Pomeron couples directly to the heavy quark loop, as shown in Fig. 1. In this paper, we will focus on the production of open heavy flavor D and B mesons and will also discuss briefly the production of nonprompt charmonia from decays of B meson. Previously, the single diffractive production for *prompt* charmonia production was studied in Refs. [4–6]. In this last case, the dominant contribution differs slightly from that of D and B mesons and is shown in the right panel of the Fig. 1. In Sec. III, we will use the results of Refs. [4–6] for comparison with our numerical results for nonprompt charmonia.

The cross section of the heavy meson production might be related to the cross section of the heavy quark production as [25–28]

$$\frac{d\sigma_M}{dyd^2p_T} = \sum_i \int_{x_Q}^1 \frac{dz}{z^2} D_i\left(\frac{x_Q(y)}{z}\right) \frac{d\sigma_{\bar{Q}_iQ_i}}{dy^* d^2p_T^*}, \qquad (1)$$

where y is the rapidity of the heavy meson (D or B meson); $y^* = y - \ln z$ is the rapidity of the heavy quark; p_T is the transverse momentum of the produced D meson; $D_i(z)$ is the fragmentation function, which describes the parton i fragmentation into a heavy meson; and $d\sigma_{\bar{Q}_iQ_i}$ is the cross section of a heavy quark production with a rapidity y^*, discussed below in Sec. II A. The dominant contribution to all heavy mesons stems from the c and b quarks (prompt and nonprompt mechanisms, respectively), so the $d\sigma_{\bar{Q}_iQ_i}$ might be evaluated in the heavy quark mass limit. The fragmentation functions for the D and B mesons, as well as

nonprompt J/ψ production, are known from the literature and for the sake of completeness are given in Appendix B.

In Fig. 1, we also included colored oval blobs, which stand schematically for the secondary interactions, which potentially could fill the large rapidity gap in the final state. The general framework for the evaluation of the rapidity gap survival factors (i.e., the probability that no particles will be produced in a rapidity gap) has been developed in Refs. [45–49], and is briefly discussed below in Sec. II B.

A. Leading-order single diffractive contribution

The single diffractive production of an on-shell heavy quark pair in the reference frame of the recoil proton might be viewed as a fluctuation of the incoming virtual gluon into a heavy $\bar{Q}Q$ pair, with subsequent *elastic* scattering of the $\bar{Q}Q$ dipole on the target proton. In perturbative QCD, the dominant contribution to such a process is given by the diagram, which includes exchange of a single Pomeron between $Q\bar{Q}$ and a recoil proton, in the spirit of the Ingelman-Schlein model [50] (see Fig. 2 for details). In LHC kinematics, the typical light-cone momentum fractions $x_{1,2}$ carried by gluons are very small ($\ll 1$), so the gluon densities are enhanced in this kinematics. This enhancement modifies some expectations based on the heavy quark mass limit. For example, there could be sizeable corrections from multiple Pomeron exchanges between the heavy dipole and the target. For this reason, instead of hard process on individual partons, it is more appropriate to use the color dipole framework (also known as CGC/Sat) [51–59]. At high energies, the color dipoles are eigenstates of interaction and thus can be used as the universal elementary building blocks automatically accumulating both the hard and soft fluctuations [60]. The light-cone color dipole framework has been developed and successfully applied to phenomenological description of both hadron-hadron and lepton-hadron collisions [61–68]. Another advantage of the CGC/Sat (color dipole) framework is that it allows a relatively straightforward extension for the description of high-multiplicity events, as discussed in Refs. [27,69–75]. The cross section of the single diffractive process, shown in Fig. 2, in the dipole approach is given by

$$\frac{d\sigma_{\bar{Q}_iQ_i}(y,\sqrt{s})}{dyd^2p_T} = \int d^2k_T x_1 g(x_1, \boldsymbol{p}_T - \boldsymbol{k}_T) \int_0^1 dz \int_0^1 dz' \times \int \frac{d^2r_1}{4\pi} \int \frac{d^2r_2}{4\pi} e^{i(\boldsymbol{r}_1-\boldsymbol{r}_2)\cdot\boldsymbol{k}_T} \times \Psi^{\dagger}_{\bar{Q}Q}(r_2,z,p_T)\Psi_{\bar{Q}Q}(r_1,z,p_T) \times N_M^{(\mathrm{SD})}(x_2(y);\vec{r}_1,\vec{r}_2) + (x_1 \leftrightarrow x_2), \quad (2)$$

$$x_{1,2} \approx \frac{\sqrt{m_M^2 + \langle p_{\perp M}^2 \rangle}}{\sqrt{s}} e^{\pm y}, \quad (3)$$

where y and $\boldsymbol{p}_T$ are the rapidity and transverse momenta of the produced heavy quark, in the center-of-mass frame of the colliding protons; $\boldsymbol{r}_1$ and $\boldsymbol{r}_2$ are the transverse distances between quark and antiquark in amplitude and its conjugate; and $\boldsymbol{k}_T$ is the transverse momentum of the heavy quark with respect to incoming gluon (namely, it is the difference between the transverse momenta of the produced quark and the incoming gluon). The latter variable equals the transverse momentum which passes through the t-channel Pomeron to the recoil proton minus the transverse momentum of undetected heavy antiquark. We also used notation $g(x_1, \boldsymbol{p}_T)$ in the first line of (2) for the unintegrated gluon PDF; $\Psi_{g\to\bar{Q}Q}(r,z)$ is the light-cone wave function of the $\bar{Q}Q$ pair with transverse separation between quarks r and the light-cone fraction of the momentum carried by the quark z. For $\Psi_{g\to\bar{Q}Q}(r,z)$, we use standard perturbative expressions [76,77],

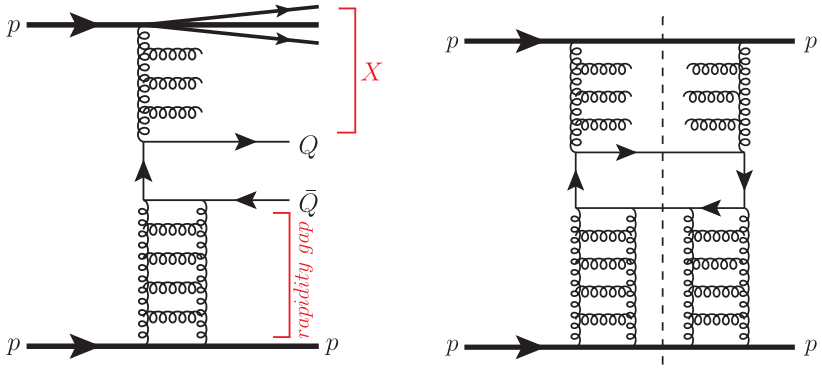

FIG. 2. Left plot: the leading-order contribution to the amplitude of single diffractive production of heavy quarks separated by a rapidity gap from the recoil proton. Right plot: illustration indicating how the cross section of the process is related to the production amplitude from three-Pomeron fusion. The dashed vertical line stands for the unitarity cut. The diagram includes one cut Pomeron (upper gluon ladder) and two uncut Pomerons (lower gluon ladders). In both plots, a summation over all possible permutations of gluon vertices in the heavy quark line/loop is implied.

$$\Psi_T^\dagger(r_2,z,Q^2)\Psi_T(r_1,z,Q^2) = \frac{\alpha_s N_c}{2\pi^2}\{\epsilon_f^2 K_1(\epsilon_f r_1)K_1(\epsilon_f r_2)[e^{i\theta_{12}}z^2 + e^{-i\theta_{12}}(1-z)^2] + m_f^2 K_0(\epsilon_f r_1)K_0(\epsilon_f r_2)\}, \quad (4)$$

$$\Psi_L^\dagger(r_2,z,Q^2)\Psi_L(r_1,z,Q^2) = \frac{\alpha_s N_c}{2\pi^2}\{4Q^2z^2(1-z)^2 K_0(\epsilon_f r_1)K_0(\epsilon_f r_2)\}, \quad (5)$$

$$\epsilon_f^2 = z(1-z)Q^2 + m_f^2, \quad (6)$$

$$|\Psi^{(f)}(r,z,Q^2)|^2 = |\Psi_T^{(f)}(r,z,Q^2)|^2 + |\Psi_L^{(f)}(r,z,Q^2)|^2, \quad (7)$$

where θ_{12} is the angle between the transverse vectors $\boldsymbol{r}_1$ and $\boldsymbol{r}_2$. The meson production amplitude N_M depends on the mechanism of the $Q\bar{Q}$ pair formation. For the case of the single diffractive production, as we demonstrate in Appendix A, the contribution to the cross section is given by

$$N_M^{(\mathrm{SD})}(x,z,\vec{\boldsymbol{r}}_1,\vec{\boldsymbol{r}}_2) \approx \int d^2\boldsymbol{b}\left[\mathcal{N}_+(x,z,\boldsymbol{r}_1,\boldsymbol{b})\left(\frac{N_c}{4}\right) + \mathcal{N}(x,\boldsymbol{r}_1,\boldsymbol{b})\left(\frac{N_c^2-4}{4N_c}+\frac{1}{6}\right)\right] \times \left[\mathcal{N}_+(x,z,\boldsymbol{r}_2,\boldsymbol{b})\left(\frac{N_c}{4}\right) + \mathcal{N}(x,\boldsymbol{r}_2,\boldsymbol{b})\left(\frac{N_c^2-4}{4N_c}+\frac{1}{6}\right)\right], \quad (8)$$

where

$$\mathcal{N}_+(x,z,\boldsymbol{r},\boldsymbol{b}) \equiv 2\mathcal{N}(x,z\boldsymbol{r},\boldsymbol{b}) + 2\mathcal{N}(x,\bar{z}\boldsymbol{r},\boldsymbol{b}) - \frac{1}{2}\mathcal{N}(x,\boldsymbol{r},\boldsymbol{b}), \quad (9)$$

and $\mathcal{N}(x,\boldsymbol{r},\boldsymbol{b})$ is the color singlet dipole cross section with explicit dependence on impact parameter $\boldsymbol{b}$.

In the heavy quark mass limit, the main contribution to the integrals in (2) comes from small dipoles of size $r \lesssim m_Q^{-1}$. In widely used phenomenological dipole parametrizations [76,78–80], it is expected that the b and r dependences factorize in this limit,

$$\mathcal{N}(x,\boldsymbol{r},\boldsymbol{b}) \approx N(x,\boldsymbol{r})T(\boldsymbol{b}), \quad (10)$$

where the transverse profile $T(b)$ is normalized as $\int d^2bT(b) = 1$, and $N(x,\boldsymbol{r})$ is the dipole cross section integrated over the impact parameter. In this approximation, we may rewrite (8) as

$$N_M^{(\mathrm{SD})}(x,z,\vec{\boldsymbol{r}}_1,\vec{\boldsymbol{r}}_2) \approx \kappa\left[N_+(x,z,\boldsymbol{r}_1)\left(\frac{N_c}{4}\right) + N(x,\boldsymbol{r}_1)\left(\frac{N_c^2-4}{4N_c}+\frac{1}{6}\right)\right] \times \left[N_+(x,z,\boldsymbol{r}_2)\left(\frac{N_c}{4}\right) + N(x,\boldsymbol{r}_2)\left(\frac{N_c^2-4}{4N_c}+\frac{1}{6}\right)\right], \quad (11)$$

where

$$N_+(x,z,\boldsymbol{r}) \equiv \int d^2b\mathcal{N}_+(x,z,\boldsymbol{r},\boldsymbol{b}) = 2N(x,z\boldsymbol{r}) + 2N(x,\bar{z}\boldsymbol{r}_1) - \frac{1}{2}N(x,\boldsymbol{r}), \quad (12)$$

$$\kappa = \int d^2\boldsymbol{b}T^2(b). \quad (13)$$

As could be seen from the structure of (8), it is a higher twist [approximately $\mathcal{O}(r^2)$] contribution compared to the amplitude of inclusive production and thus should have stronger suppression at large p_T.

The p_T-integrated cross section gets contributions only from dipoles with $\vec{\boldsymbol{r}}_1 = \vec{\boldsymbol{r}}_2 = \vec{\boldsymbol{r}}$ in the integrand. For this case, it is possible to show that the gluon uPDF $x_1 g(x_1, \boldsymbol{p}_T - \boldsymbol{k}_T)$ is replaced with the integrated gluon PDF $x_g G(x_g,\mu_F)$ taken at the scale $\mu_F \approx 2m_Q$. In the LHC kinematics at central rapidities, this scale significantly exceeds the saturation scale $Q_s(x)$, which justifies the dominance of the three-Pomeron approximation. However, in the small-x kinematics, there are sizeable nonlinear corrections to the evolution in the dipole approach. In this kinematics, the corresponding scale μ_F should be taken at the saturation momentum Q_s. The gluon PDF $x_1 G(x_1,\mu_F)$ in this approach is closely related to the dipole scattering amplitude $N(x,\boldsymbol{r}) = \int d^2bN(x,\boldsymbol{r},\boldsymbol{b})$ as [69,81]

$$\frac{C_F}{2\pi^2\bar{\alpha}_S}N(x,\boldsymbol{r}) = \int\frac{d^2k_T}{k_T^4}\phi(x,\boldsymbol{k}_T)(1-e^{i\boldsymbol{k}_T\cdot\boldsymbol{r}}); \qquad xG(x,\mu_F) = \int_0^{\mu_F}\frac{d^2k_T}{k_T^2}\phi(x,\boldsymbol{k}_T); \quad (14)$$

Eq. (14) can be inverted and gives the gluon uPDF in terms of the dipole amplitude,

$$xG(x,\mu_F) = \frac{C_F\mu_F}{2\pi^2\bar{\alpha}_S}\int d^2r\frac{J_1(r\mu_F)}{r}\nabla_r^2 N(x,\boldsymbol{r}). \quad (15)$$

The corresponding unintegrated gluon PDF can be rewritten as [82]

$$xg(x,k^2) = \frac{\partial}{\partial \mu_F^2} xG(x,\mu_F)\Big|_{\mu_F^2=k^2}, \tag{16}$$

which allows ua to express the single diffractive cross section in terms of only the dipole amplitude. The expression (16) will be used below in Sec. IV for extension of our results to high-multiplicity events.

B. Gap survival factors

The rapidity gap between the recoil proton and the produced heavy meson might be filled potentially by products of various secondary processes, as shown schematically by the colored vertical and inclined ovals in Fig. 1. As was demonstrated in Refs. [45–48], the effect of these factors is significant at high energies and might decrease the observed yields (i.e., probability of nonobservation of particles in the gap) by more than an order of magnitude [48,49]. This suppression is due to soft interactions between the colliding protons and thus is not related to the particles produced due to hard interactions. The evaluation of this suppression conventionally follows the ideas of Good and Walker [83], which are usually implemented in the context of different models (see for review Refs. [84–87]). Technically, all these approaches perform evaluations in the eikonal approximation and predict that the observables, which include large rapidity gaps, are suppressed by a so-called gap survival factor,

$$\langle S^2 \rangle = \frac{\int d^2b |\mathcal{M}(b,s,\ldots)|^2 \exp\left(-\hat{\Omega}(b,s)\right)}{\int d^2b |\mathcal{M}(b,s,\ldots)|^2}, \tag{17}$$

where $\mathcal{M}(b,s,\ldots)$ is the amplitude of the hard process, b is the impact parameter, and Ω is the opacity or optical density. In a single-channel eikonal model, the opacity Ω is directly related to the cross sections of total, elastic, and inelastic processes [85]. It is expected that the energy dependence of the function Ω is controlled by the Pomeron intercept, $\Omega \sim s^{\alpha_{\mathrm{IP}}-1}$, so the factor (17) decreases as a function of energy. The single-channel model is very simple, yet its predictions are in tension with experimental data [49]. A more accurate description of data is achieved in multichannel extensions of these models, which assume that after interaction with a soft Pomeron the proton might convert into additional $N_D - 1$ diffractive states. In this basis, the soft Pomeron interaction amplitude $\hat{\Omega}$ should be considered as an $N_D \times N_D$ matrix. As was discussed in Refs. [84–86], for a good description, it is sufficient to choose $N_D = 2$, with the common parametrization for the matrix Ω_{ik} given in Ref. [88] and briefly summarized for the sake of completeness in Appendix C. For the single diffractive scattering, the exponent in the expression (17) should be understood as a matrix element between $|pp\rangle$ and $|pX\rangle$ states [89,90]. If Φ_1 and Φ_2 are eigenvalues of Ω_{ik} with eigenvalues Ω_1 and Ω_2, then the matrix $\exp\left(-\hat{\Omega}(b,s)\right)$ reduces in this basis to a linear combination of factors approximately $e^{-\Omega_a(s,b)}$, in which the coefficients can be fixed by projecting the proton and diffractive states onto the eigenstates Φ_1, Φ_2 of the scattering matrix. For the single diffractive production, the algorithm for evaluation of the survival factor was introduced earlier for the $pp \to pX$ process in Ref. [90], yielding

$$\begin{aligned}\exp\left(-\hat{\Omega}(b,s)\right) &\to \mathcal{S}^2(s_{pp},b) \\ &\equiv \frac{1}{4(1+\lambda^2)}\left((1+\lambda)^3 e^{-(1+\lambda)^2\Omega} + (1-\lambda)^3 e^{-(1-\lambda)^2\Omega}\right. \\ &\quad \left. + 2(1-\lambda^2)e^{-(1-\lambda^2)\Omega}\right),\end{aligned} \tag{18}$$

where parameter Ω is related to eigenvalues $\Omega_{1,2}$ of the matrix Ω_{ik} as

$$\Omega = \frac{\Omega_1 + \Omega_2}{2} \tag{19}$$

and the parameter λ stands for the ratio of the production amplitude of diffractive state X to the amplitude of elastic proton scattering of the incident proton on a Pomeron. Currently, there are two widely used parametrizations of Ω_{ik} available from the literature, the so-called Durham model [46,49,86,89,90] (see the short summary in Appendix C) and the so-called GLM parametrization [84,85]. In Fig. 3, we have shown the dependence of the gap survival factor $\mathcal{S}^2$ on the impact parameter b of the collision, evaluated with both parametrizations. As we can see, the suppression is maximal ($\mathcal{S} \ll 1$) for collisions with small impact parameter b. In the opposite limit of large b, the matrix $\hat{\Omega}(b,s)$ as well as its eigenvalues are suppressed, and for this reason, suppression is weak, and $\mathcal{S}$ approaches unity. We can see that the shapes of the curves are close to

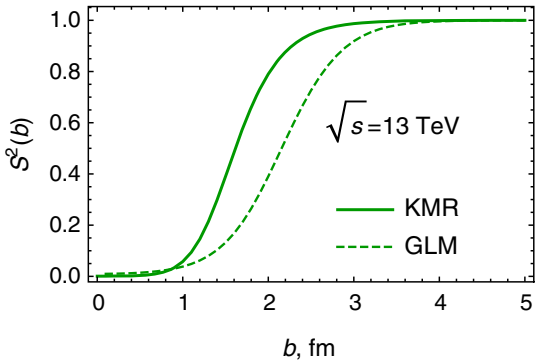

FIG. 3. The gap survival factor as defined in (18). The label "KMR" is used for $\mathcal{S}^2$ evaluated with parametrization of Khoze-Martin-Ryskin from Refs. [46,49,86,89,90], also known as the "Durham model" (see a short summary in Appendix C). This parametrization is used for all further evaluations. The label "GLM" is used for $\mathcal{S}^2$ evaluated with parametrization from Refs. [84,85].

each other, and therefore we expect that predictions for physical observables made with them should coincide within a factor of 2. For our evaluations, we prefer to use the Durham model, since its most recent versions are based on recent diffractive data from the LHC.

In this paper, we are interested only in events without charged particles, produced at pseudorapidity $\eta < y$ (rapidity gap between the recoil proton and heavy quarks), whereas the evaluation of the survival factor in (17), (18), and (21) was performed under the assumption that there are no coproduced particles in the whole rapidity range $\eta \in (-y_{\max}, y_{\max})$, which is much stricter than needed in this problem. For this reason, we need to correct the estimate (18), using probabilistic considerations. In what follows, we will use notations P_A and P_B for the probabilities to emit at least one charged particle in the intervals $\eta < y$ and $\eta > y$ due to soft interaction of the colliding protons, while $\bar{P}_A \equiv 1 - P_A$ and $\bar{P}_B \equiv 1 - P_B$ are the probabilities not to emit any particles in these intervals (the gap survival factors on these intervals). We will also use the notation $\bar{P}_{A\cup B}$ for the probability not to produce particles in any of the intervals. The relation between the probabilities $\bar{P}_{A\cup B}$ and $\bar{P}_A$, $\bar{P}_B$ depends crucially on possible correlations between particles from different rapidity intervals. Such correlations have been studied in the literature [91–93], and it is known that they are small when the separation between the bins is larger than 1–2 units in rapidity. If we neglect completely such correlations, the probabilities are related as $\bar{P}_{A\cup B} = \bar{P}_A \bar{P}_B$, which implies that the survival factor should scale with the length of the rapidity bin as $S^2(\Delta\eta) \sim \text{const}^{\Delta\eta}$. For the single diffractive production of heavy mesons, we require that no particles are produced with $\eta < y$, although we do not impose any conditions for $\eta > y$ (so we do not need to introduce the gap survival factor in this region). This implies that the overall survival factor (18) should be adjusted as

$$\mathcal{S}^2 \to S^2(s_{pp}, b) = (\mathcal{S}^2)^{\frac{\Delta y}{2y_{\max}}} \gtrsim \mathcal{S}^2, \tag{20}$$

where Δy is the width of the rapidity gap interval and $y_{\max} = -\frac{1}{2}\ln(m_{Q,T}^2/s)$ is the largest possible rapidity of heavy quarks. This factor $S^2(s_{pp}, b)$ should be included into the expressions (2) and (8) from the previous Sec. II A.

In the heavy quark mass limit, the dipoles are small, $r \lesssim m_Q^{-1}$, and we may use a factorized approximation (10). The convolution of $S^2(s_{pp}, b)$ with impact parameter dependent cross section can be simplified in this limit and yields for the suppression factor a much simpler expression,

$$\langle S^2 \rangle \approx \frac{\int d^2b T^2(b) S^2(s_{pp}, b)}{\int d^2b T^2(b)}, \tag{21}$$

which depends only on the energy (Mandelstam variable) s_{pp} of the collision but does not depend on masses nor kinematics of the produced heavy quarks.

III. NUMERICAL RESULTS

For our numerical evaluations here and in what follows, we will we use the impact parameter (b) dependent "bCGC" parametrization of the dipole cross section [79,80]

$$N(x, \boldsymbol{r}, \boldsymbol{b}) = \begin{cases} N_0\left(\frac{rQ_s(x)}{2}\right)^{2\gamma_{\text{eff}}(r)}, & r \le \frac{2}{Q_s(x)} \\ 1 - \exp\left(-\mathcal{A}\ln(\mathcal{B}rQ_s)\right), & r > \frac{2}{Q_s(x)} \end{cases}, \tag{22}$$

$$\mathcal{A} = -\frac{N_0^2\gamma_s^2}{(1-N_0)^2\ln(1-N_0)}, \qquad \mathcal{B} = \frac{1}{2}(1-N_0)^{-\frac{1-N_0}{N_0\gamma_s}}, \tag{23}$$

$$Q_s(x, \mathbf{b}) = \left(\frac{x_0}{x}\right)^{\lambda/2} T_G(b),$$
$$\gamma_{\text{eff}}(r) = \gamma_s + \frac{1}{\kappa\lambda Y}\ln\left(\frac{2}{rQ_s(x)}\right), \tag{24}$$

$$\gamma_s = 0.66, \qquad \lambda = 0.206, \qquad x_0 = 1.05 \times 10^{-3},$$
$$T_G(b) = \exp\left(-\frac{b^2}{2\gamma_s B_{\text{CGC}}}\right). \tag{25}$$

In Figs. 4, 5, and 6, we show the production cross sections of the D mesons, B mesons, and nonprompt J/ψ mesons. We can see that in the small-p_T region, which encompasses most of the events, the single-diffraction production constitutes approximately 1% of the inclusive cross section. In the large-p_T region, the contribution from the single diffractive production is strongly suppressed since it is formally a higher twist effect.

To the best of our knowledge, there is no direct experimental data for the cross sections of the suggested process. The diffractive production of B mesons was studied earlier by the CDF Collaboration in Ref. [16], although the results are only available for the ratio of the integrated cross sections of diffractive and inclusive processes,

$$R_{\bar{b}b}^{(\text{diff.})}(s) \equiv \frac{\sigma_{B^+}^{\text{diff}}(s)}{\sigma_{B^+}^{\text{incl}}(s)}. \tag{26}$$

For energy $\sqrt{s} = 1.8$ TeV, it was found that

$$R_{\bar{b}b}^{(\text{diff.})}(\sqrt{s} = 1.8\ \text{TeV}) = (0.62 \pm 0.19 \pm 0.16)\%. \tag{27}$$

In Table I, we present our theoretical expectations for this value. For Tevatron kinematics, the model prediction

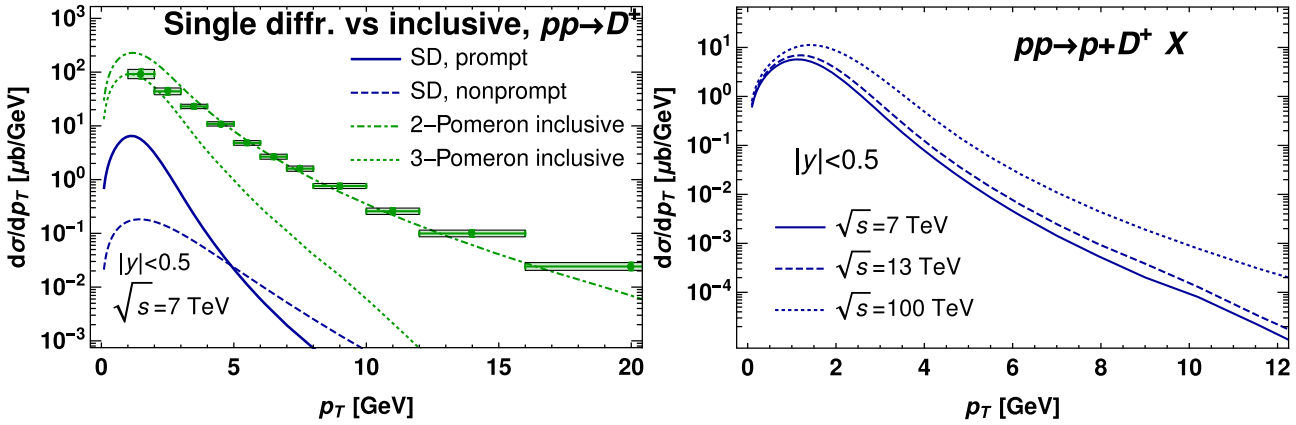

FIG. 4. The cross section $d\sigma/dp_T$ of the single diffractive production of D^+ mesons. Integration over the rapidity bin $|y| < 0.5$ is implied. Left plot: comparison with inclusive production in the LHC kinematics for $\sqrt{s} = 7$ TeV (theory and experiment). The curves with labels "SD, prompt" and "SD, nonprompt" correspond to single diffractive contributions to D meson yields from the fragmentation of the c and b quarks, respectively. The curves marked "2-Pomeron inclusive" and "3-Pomeron inclusive" stand for the contributions of two- and three-Pomeron fusion mechanisms to inclusive D meson yields, respectively (see a short overview in Appendix A 2 and more detailed discussion in Ref. [41]). The experimental data are for inclusive production from Ref. [94]. Right plot: $\sqrt{s}$ dependence of the data in the kinematics of LHC and the planned Future Cicular Collider (FCC) [95]. For other D mesons the p_T dependence has a very similar shape, yet differs numerically by a factor of 2.

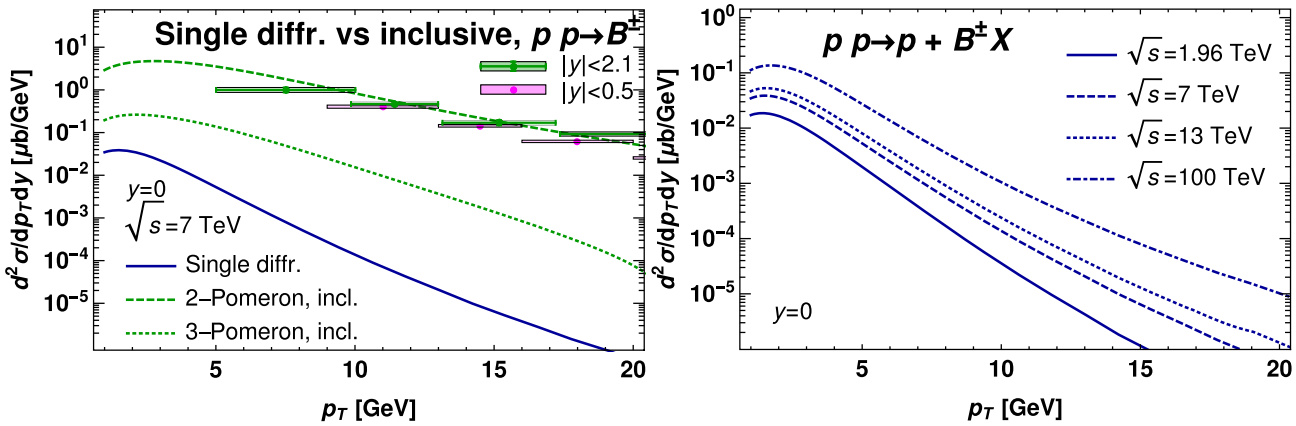

FIG. 5. Cross section for the single diffractive $B^{\pm}$ mesons production. Left plot: comparison of single diffractive predictions with inclusive cross sections (experimental and theoretical results). The theoretical curves marked "2-Pomeron incl." and "3-Pomeron incl." stand for the additive contributions from two- and three-Pomeron fusion mechanisms, respectively (see Ref. [41] and a short discussion in Appendix A 2).The experimental data are for inclusive production from CMS [96] ("$|y| < 2.1$" data points) and ATLAS [97] ("$|y| < 0.5$" data points). For some experimentally measured results, bin-integrated cross sections $d\sigma/dp_T$ was converted into $d\sigma/dp_T dy$ dividing by the width of the rapidity bin (this is justified since in LHC kinematics at central rapidities $y \approx 0$ the cross section is flat). Right plot: the p_T dependence of the cross section $d\sigma/dydp_T$ for several energies $\sqrt{s}$.

$R_{\bar{b}b}^{(\mathrm{diff.})} \approx 0.4\%$ agrees with (27), within uncertainty of experimental data (27). As we can see from the same table, in LHC kinematics, the ratio (26) is approximately of the same order. The smallness of the values in Table I is due to the fact that the production of a heavy quark in single-diffraction events is formally a higher twist effect and thus has an additional suppression by the factor approximately $(\Lambda_{\mathrm{QCD}}/m_Q)^2$. While the absolute cross sections of single diffractive and inclusive production increase as a function of energy, the ratio (27) slowly *decreases* due to energy dependence of the gap survival factor in single diffractive cross section.

We extended the definition (26) and analyzed the ratio of differential cross sections,

$$R_M^{(\mathrm{diff.})}(s,y,p_T) \equiv \frac{d\sigma_M^{\mathrm{diff}}/dydp_T}{d\sigma_M^{\mathrm{incl}}/dydp_T}, \quad M = D^{\pm}, B^{\pm}, \ldots, \qquad (28)$$

which presents a novel observable. In Fig. 7, we show this ratio as a function of p_T for D mesons, both for prompt and nonprompt mechanisms. For the sake of definiteness, we

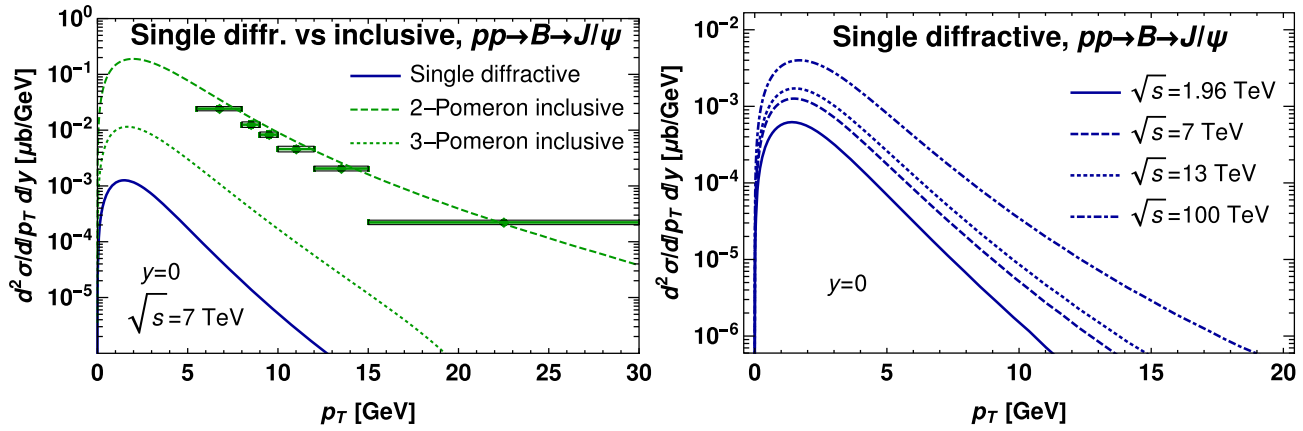

FIG. 6. Cross section for the single diffractive nonprompt J/ψ mesons production. Left plot: comparison of single diffractive predictions with inclusive cross sections (experimental and theoretical results). The theoretical curves marked "2-Pomeron inclusive" and "3-Pomeron inclusive" stand for the additive contributions from two- and three-Pomeron fusion mechanisms, respectively (see Ref. [41] and a short discussion in Appendix A 2).The experimental data are for inclusive production from CMS [98]. Right plot: the p_T dependence of the cross section $d\sigma/dydp_T$ for several energies $\sqrt{s}$.

considered D^+ mesons, although the results for the ratio (28) are almost the same for other choices of D mesons. In Fig. 8, we show the same ratio for the B mesons (B^+ for definiteness) and nonprompt J/ψ. We can see that the ratio is smaller than for D mesons and decreases quite fast at large p_T. This behavior agrees with our earlier observation that the single diffractive mechanism is formally a higher twist effect compared to the dominant two-gluon fusion mechanism, in the case of inclusive production. As expected, at small p_T, the ratios are similar for B mesons and nonprompt J/ψ; for larger p_T, the results differ due to differences in fragmentation functions (see Appendix B for details).

In Fig. 9, we compare our results for nonprompt production of J/ψ with the predictions for prompt production from Refs. [5,6] (color octet contributions + gluon fragmentation, dominant at large p_T) and from Ref. [4] (color evaporation model). As we can expect, the nonprompt mechanism is smaller than the prompt contribution, although the qualitative behavior is similar in both cases.

In Fig. 10, we compare our predictions with earlier results from Refs. [11,12] obtained in the framework of the Ingelman-Schlein model [50]. We can see that in the region $p_T \lesssim 5$ GeV, where the majority of heavy mesons is produced, all approaches give comparable contributions. At larger p_T, the discrepancy between the different approaches increases. Our results in this kinematics are close to predictions in the collinear framework evaluation, presented in Ref. [11] and differ quite substantially from the results of Ref. [12] found in the k_T-factorization framework by the same group.

Finally, we would like to stop briefly on the ratio $R^{(\mathrm{diff})}_{J/\psi}$ of single diffractive and inclusive contributions. It was predicted in Ref. [6] that for the prompt contributions $R^{(\mathrm{diff,prompt})}_{J/\psi} \approx 0.65 \pm 0.15\%$, although later the CDF Collaboration [15] found a value twice larger:

$$R^{(\mathrm{diff,\,CDF})}_{J/\psi} \approx 1.45 \pm 0.25\%. \tag{29}$$

This mismatch might be explained by sizeable nonprompt contributions: combining $R^{(\mathrm{diff,\,prompt})}_{J/\psi}$ with $R^{(\mathrm{diff,\,non\text{-}prompt})}_{J/\psi}$ from the first line in Table I, we get $R^{(\mathrm{diff,\,prompt+nonprompt})}_{J/\psi} \approx$ 1.22%, in reasonable agreement with the experimental value (29).

TABLE I. Values of the ratio of single diffractive and inclusive productions cross sections, as defined in (26), in Tevatron and LHC kinematics. The second and the third columns correspond to the c and b quarks ($R^{(\mathrm{diff})}_{\bar{c}c}$ and $R^{(\mathrm{diff})}_{\bar{b}b}$, respectively). The last column $R^{(\mathrm{diff})}_{J/\psi}$ is for the nonprompt J/ψ production.

$\sqrt{s}$ (TeV)	$R^{(\mathrm{diff})}_{\bar{c}c}$ (%)	$R^{(\mathrm{diff})}_{\bar{b}b}$ (%)	$R^{(\mathrm{diff})}_{J/\psi}$ (%)
1.8	2.20	0.40	0.57
7	1.87	0.33	0.45
13	1.59	0.30	0.40

IV. MULTIPLICITY DEPENDENCE

According to the Local Parton Hadron Duality hypothesis [99–101], the multiplicity of produced hadrons in a given event is directly related to the number of partons produced in a collision. For this reason, the study of multiplicity dependence of different processes presents an interesting extension, which allows us to understand better the onset of the saturation regime in high-energy collisions. A feasibility to measure such processes was demonstrated for inclusive channels by the STAR [33,34]

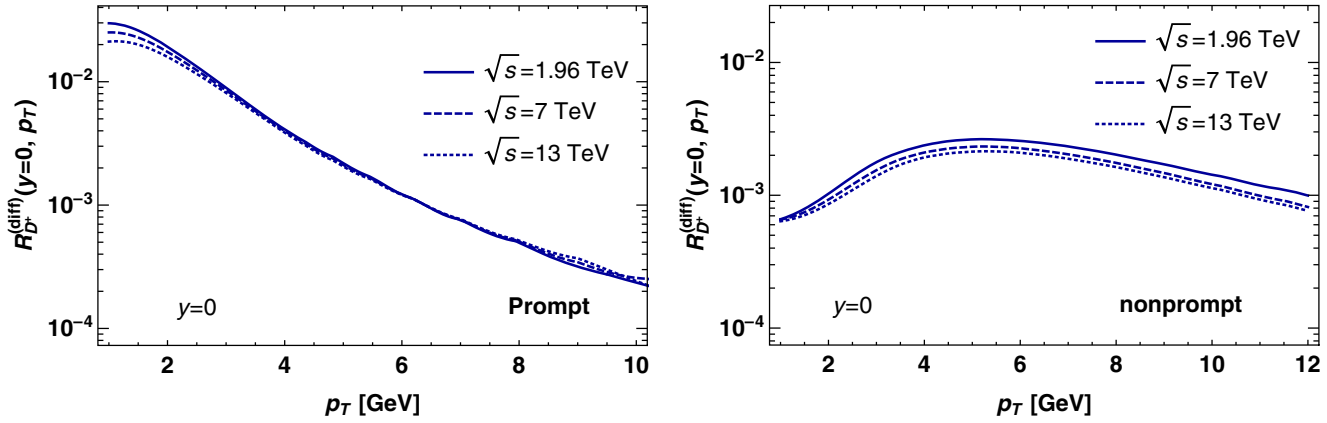

FIG. 7. The ratio of single diffractive to inclusive production cross sections, as defined in (28). The left plot corresponds to the prompt production (from $c \to D$ fragmentation), and the right plot is for the nonprompt mechanism (from $b \to D$ fragmentation). For the sake of definiteness, we considered D^+ mesons; for other D mesons, the results have a very similar shape.

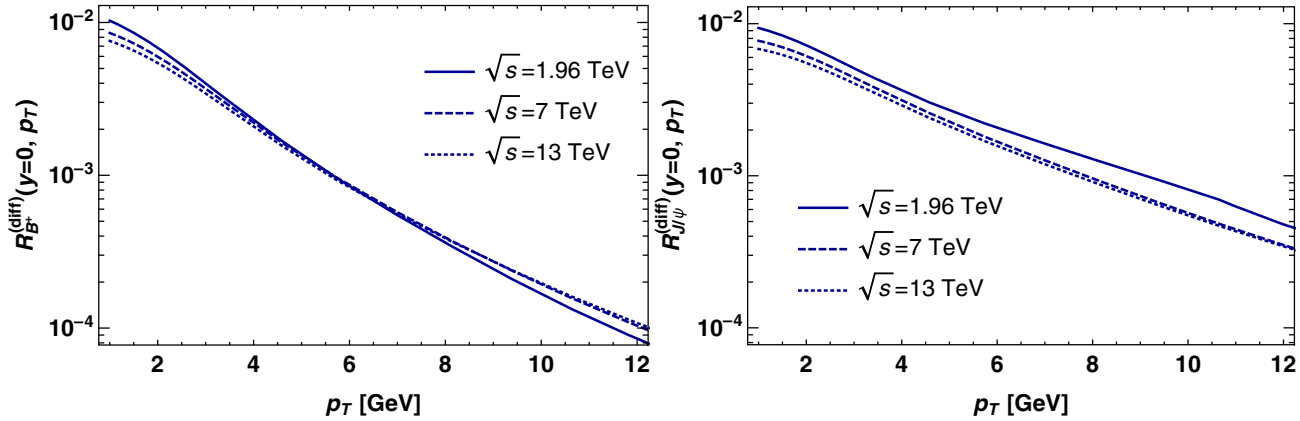

FIG. 8. The ratio of single diffractive to inclusive production cross sections, as defined in (28). The left plot is for the B mesons, and the right panel is for nonprompt production of J/ψ mesons.

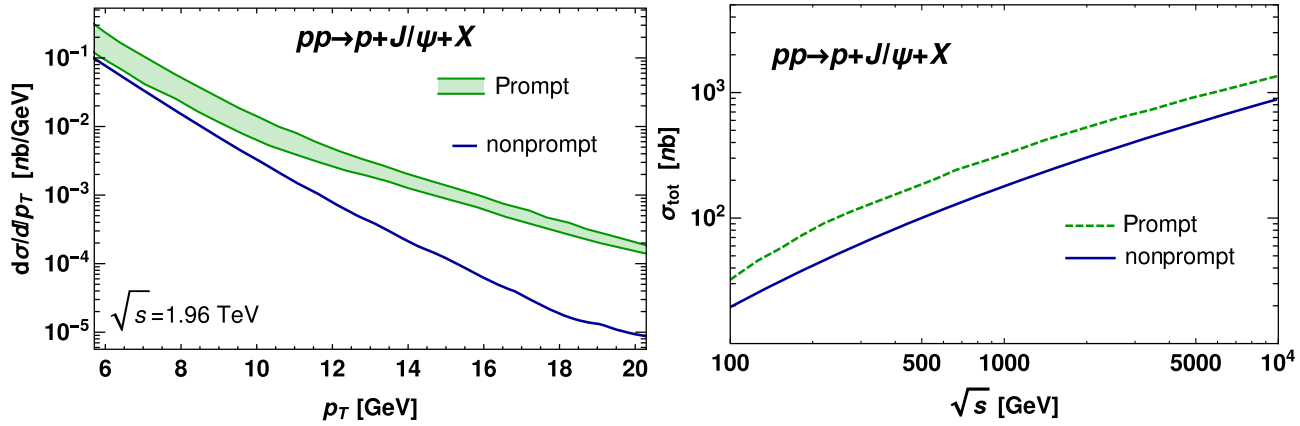

FIG. 9. Left plot: p_T dependence of differential cross sections of prompt and nonprompt mechanisms for single diffractive production of J/ψ mesons. The results for the prompt mechanism are taken from Refs. [5,6], and the width of the green band reflects the uncertainty due to one of the model parameters (gluon fraction of Pomeron f_g). The results for the nonprompt mechanism (blue solid curve) are results of this paper. Right plot: energy dependence of total cross sections of prompt and nonprompt single diffractive production mechanisms of J/ψ mesons. The prompt contribution (green dashed line) is taken from Ref. [4].

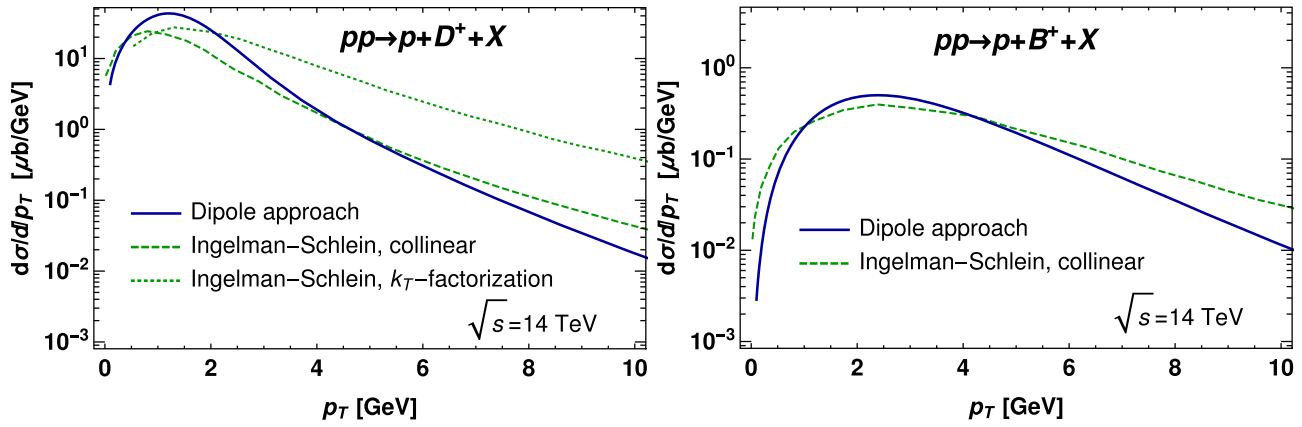

FIG. 10. Comparison of color dipole approach predictions (this paper) with results of Refs. [11,12] obtained in the framework of Ingelman-Schlein model [50]. The left plot corresponds to single diffractive charm production, the right plot is for bottom quarks. Our predictions are marked with label "Dipole approach". The results of Ref. [11] are marked with label "Ingelman-Schelin, collinear," and the results of Ref. [12] are marked as "Ingelman-Schlein, k_T-factorization."

and ALICE [32,102] collaborations. The extension of these experimental measurements to single diffractive production is quite straightforward, since their detectors have the capability to detect simultaneously both the rapidity gaps and the charged particles outside of the rapidity window. Since the cross section of single diffractive production is significantly smaller than that of inclusive production, and the probability of events with large multiplicity is exponentially suppressed [102], each measurement will require larger integrated luminosity.

To get rid of a common exponential suppression at large multiplicities, for a comparison of the multiplicity dependence in different channels, it is widely accepted to use a self-normalized ratio [103],

$$\frac{dN_M/dy}{\langle dN_M/dy\rangle} = \frac{w(N_M)}{\langle w(N_M)\rangle}\frac{\langle w(N_{\rm ch})\rangle}{w(N_{\rm ch})} = \frac{d\sigma_M(y,\eta,\sqrt{s},n)/dy}{d\sigma_M(y,\eta,\sqrt{s},\langle n\rangle=1)/dy}\Big/\frac{d\sigma_{\rm ch}(\eta,\sqrt{s},Q^2,n)/d\eta}{d\sigma_{\rm ch}(\eta,\sqrt{s},Q^2,\langle n\rangle=1)/d\eta}, \tag{30}$$

where $\langle N_{\rm ch}\rangle = \Delta\eta dN_{\rm ch}/d\eta$ is the average number of particles detected in a given pseudorapidity window $(\eta-\Delta\eta/2,\eta+\Delta\eta/2)$, $n = N_{\rm ch}/\langle N_{\rm ch}\rangle$ is the relative enhancement of the number of charged particles in the same pseudorapidity window, $w(N_M)/\langle w(N_M)\rangle$ and $w(N_{\rm ch})/\langle w(N_{\rm ch})\rangle$ are the self-normalized yields of heavy meson M ($M = D, B$) and charged particles (minimal bias events) in a given multiplicity class, $d\sigma_M(y,\sqrt{s},n)$ is the production cross sections for heavy meson M with rapidity y and $N_{\rm ch} = n\langle N_{\rm ch}\rangle$ charged particles in the pseudorapidity window $(\eta-\Delta\eta/2,\eta+\Delta\eta/2)$, and $d\sigma_{\rm ch}(y,\sqrt{s},n)$ is the production cross sections for $N_{\rm ch} = n\langle N_{\rm ch}\rangle$ charged particles in the same pseudorapidity window. Mathematically, the ratio (30) gives a *conditional* probability to produce a meson M in a single diffractive collision in which $N_{\rm ch}$ charged particles are produced.

In the color dipole (CGC/Sat) approach, the framework for description of the high-multiplicity events has been developed in Refs. [27,69–75]. In this picture, the observation of enhanced multiplicity signals that a larger than average number of partons is produced in a given event. Nevertheless, we still expect that each Pomeron should satisfy the nonlinear Balitsky-Kovchegov equation. The bCGC dipole amplitude (22) was constructed as an approximate solution of the latter, and for this reason, it should maintain its form, although the value of the saturation scale Q_s might be modified. As was demonstrated in Refs. [69–71], the observed number of charged multiplicity $dN_{\rm ch}/dy$ of soft hadrons in pp collisions is proportional to the saturation scale Q_s^2 (modulo logarithmic corrections), and for this reason, the events with large multiplicity might be described in dipole framework by simply rescaling Q_s^2 as a function of n [69–75],

$$Q_s^2(x,b;n) = nQ^2(x,b). \tag{31}$$

It was demonstrated in Ref. [27] that the error of the approximation (31) is less than 10% in the region of interest ($n \lesssim 10$), and for this reason, we will use it for our estimates. While at LHC energies it is expected that the typical values of saturation scale $Q_s(x,b)$ fall into the range 0.5–1 GeV, from (31), we can see that in events with enhanced multiplicity this parameter might exceed the values of heavy quark mass m_Q and lead to an interplay of large-Q_s and large-m_Q limits. The expression (31) explicitly illustrates that the study of the high-multiplicity

events gives us access to a new regime, which otherwise would require significantly higher energies.

The observation of enhanced multiplicity in the process shown in the left diagram of Fig. 1 implies that unintegrated gluon density $g(x,\boldsymbol{k}_\perp,n)$ in (2) is also modified. This change might be found by taking into account the relation of gluon density with the dipole amplitude $N(x,r,b)$ given by (16). For the sake of simplicity below, we will focus on the multiplicity dependence of the p_T-integrated cross section, which is easier to measure experimentally. For this case, the cross section (2) simplifies considerably, since, after integration over p_T, the multiplicity dependent (integrated) gluon density factorizes and contributes to the result as a multiplicative factor. For this reason, the ratio (30) reduces to a common factor,

$$\frac{dN_M/dy}{\langle dN_M/dy\rangle}=\frac{\int d^2r\frac{J_1(r\mu_F)}{r}\nabla_r^2N(y,\boldsymbol{r},n)}{\int d^2r\frac{J_1(r\mu_F)}{r}\nabla_r^2N(y,\boldsymbol{r},1)}, \tag{32}$$

the same for all mesons. In Fig. 11, we show the multiplicity dependence of the ratio (32). At very small n, when saturation effects are small, the size of the dipole is controlled by the mass of heavy quark approximately $1/m_Q$, and thus the dipole amplitude $N(y,\boldsymbol{r},n)$ might be approximated as $N(y,\boldsymbol{r},n)\sim(rQ_s(y,n))^\gamma$, where $\gamma\approx 0.63$–0.76 is a numerical parameter. In view of (31), this translates into the multiplicity dependence

$$\frac{dN_M/dy}{\langle dN_M/dy\rangle}\sim n^\gamma, \tag{33}$$

as shown in the same figure with red dotted line. At larger values of n, due to saturation effects, the curve deviates from the small-n asymptotic behavior. As we can see from the right panel of the same figure, this behavior is different from the dependence seen by ALICE for *inclusive* the production [32], as well as from our theoretical result for inclusive production from Ref. [41]. This happens because in single diffractive production the coproduced hadrons stem from only one cut Pomeron, whereas in inclusive production, in the setup studied in Ref. [32], at least two Pomerons can contribute to the observed multiplicity enhancement. Since each cut Pomeron gives a factor approximately n^γ in multiplicity dependence, this explains the predicted difference between the single diffractive and inclusive processes.

V. NUCLEAR EFFECTS

The study of the single diffractive production on nuclear collisions is appealing because its cross section grows rapidly with atomic number A, and thus is easier to measure experimentally. The AA collisions are not suitable for this purpose due to formation of hot quark-gluon plasma at later stages [104–110]. For this reason, we will focus on pA collisions and in the kinematics when the scattered proton in the final state is separated by large rapidity gap from the produced heavy meson and nuclear debris. The framework for studying the opposite limit (when the *nucleus* is separated by the rapidity gap from other hadrons) might be found in Refs. [111,112].

In the literature, there are two conceptually different frameworks for description of nuclear effect. In the Gribov-Glauber approach [113–115], the nuclear cross section is related to that of individual nucleons, and thus each nucleon contributes to the scattering cross section. In this picture, we should take into account that the nucleus is an extended object, and at very high energies, a heavy quark dipole might interact with more than one nucleon during its

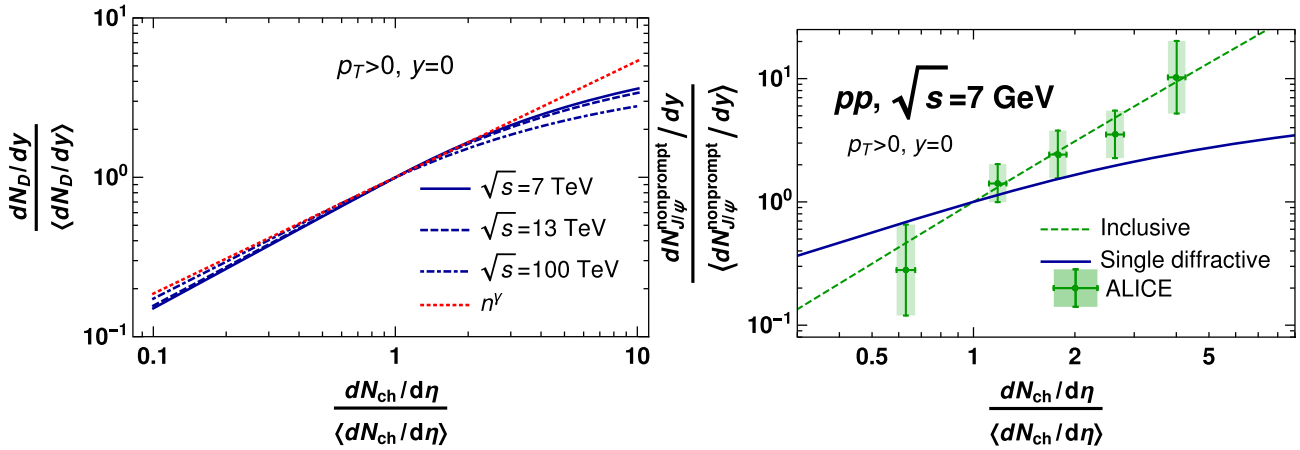

FIG. 11. Left plot: multiplicity dependence of open heavy flavor meson production cross sections with single diffractive mechanism (the same for all mesons; see the text for explanation). The red dotted line corresponds to the asymptotic expression for small multiplicities, as explained in the text. Right plot: comparison of multiplicity dependence for inclusive and single diffractive production for nonprompt J/ψ mesons. The experimental points are from ALICE [32] for inclusive production, and the theoretical curve for inclusive production is from Ref. [41].

propagation. However, there is a plethora of new effects which should be taken into account [116–119]. In CGC approach, which is valid at very high energies, all hadrons are described as color glass condensate. All the interactions of a dipole with a target (nucleus) are encoded in a color dipole cross section $N_A(x,\boldsymbol{r},\boldsymbol{b})$. Since the latter should satisfy the same Balitsky-Kovchegov equation as for proton, the functional form of $N_A(x,\boldsymbol{r},\boldsymbol{b})$ should be similar to (22). In this approach, the nucleus differs from the proton by larger size $R_A = A^{1/3}R_p$ and larger values of the saturation scale Q_{sA}^2. As was found in Refs. [120,121] from analysis of the experimental data, the dependence of Q_{sA}^2 on atomic number A might be approximated by

$$Q_{sA}^2(x) \approx Q_s^2(x)A^{1/3\delta} \qquad \delta \approx 0.79 \pm 0.02. \tag{34}$$

The value $\delta < 1$ indicates that the saturation scale grows *faster* than approximately $A^{1/3}$ expected from naive geometric estimates. In the single diffractive process, the nucleus contributes in (2) only through the unintegrated gluon density $g(x,\boldsymbol{k})$. Currently, the latter is poorly defined experimentally [118], and for this reason, we will estimate it from the dipole amplitude using (15) and (16). The magnitude of nuclear effects is conventionally expressed in terms of the normalized ratio of the cross sections on the nucleus and proton,

$$R_A(y) = \frac{d\sigma_{pA\to pMX}/dy}{Ad\sigma_{pp\to pMX}/dy}. \tag{35}$$

For the sake of simplicity, we will focus on the p_T-integrated cross section. In this case, the dependence on the gluon PDF factorizes, and thus the ratio (35) reduces to a common prefactor,

$$R_A(y) \approx \frac{g_A(x_1(y),\mu_F)}{g_N(x_1(y),\mu_F)} = \frac{1}{A}\frac{\int d^2b \int d^2r \frac{J_1(r\mu_F)}{r}\nabla_r^2 N_A(y,\boldsymbol{r},\boldsymbol{b}/A^{1/3})}{\int d^2b \int d^2r \frac{J_1(r\mu_F)}{r}\nabla_r^2 N(y,\boldsymbol{r},\boldsymbol{b})}, \tag{36}$$

where $N_A(y,\boldsymbol{r},\boldsymbol{b})$ is a nuclear dipole amplitude with adjusted saturation scale (34) and the rescaling of the impact parameter $\boldsymbol{b}$ in the numerator reflects the increase of the nuclear radius. In Fig. 12, we have shown the ratio (35) as a function of the atomic number A. We can see that, due to nuclear (saturation) effects, the cross section decreases by up to a factor of 2 for very heavy nuclei. This finding is in agreement with expected suppression of nuclear gluon densities found in Ref. [118] from global fits of experimental data.

Finally, from comparison of (32) and (36), we may obtain the relation between the *nuclear* suppression factor

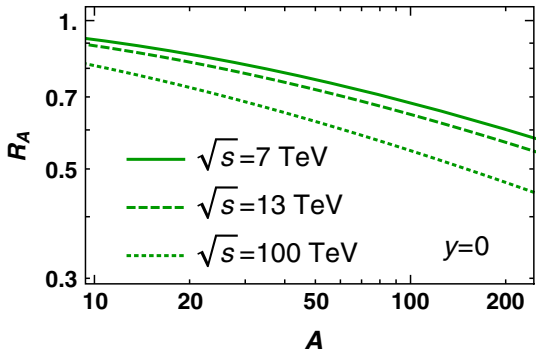

FIG. 12. The nuclear suppression factor R_A defined in (35) as a function of the atomic number A for the p_T-integrated cross section (the same for all mesons; see the text for explanation).

R_A and the multiplicity dependence of the *proton* cross section (32),

$$AR_A(y,A) = \left.\frac{dN_M/dy}{\langle dN_M/dy\rangle}\right|_{n=(Q_{sA}^2/Q_s^2)},$$

which might be checked experimentally.

VI. CONCLUSIONS

In this paper, we studied single diffractive production of open heavy flavor mesons. We analyzed in detail the production of D and B mesons, as well as nonprompt production of J/ψ mesons. While in general diffractive events constitute up to 20% of the inclusive cross section [1], we found that for heavy mesons production the single diffractive events constitute only 0.4%–2% of all inclusively produced heavy mesons. This happens because the leading-order contribution to single diffractive production is formally a higher twist effect (compared to leading-order inclusive diagrams) and thus includes additional suppression approximately $(\Lambda_{\rm QCD}/m_Q)^2$. Similarly, the observed suppression at large transverse momentum p_T of the produced heavy meson agrees with expected pattern of higher twist suppression. Nevertheless, we believe that the cross sections are sufficiently large and thus could be measured with reasonable precision at the LHC.

We also analyzed the dependence on multiplicity of coproduced hadrons, assuming that these are produced only on one side of the heavy meson. We found that the dependence on multiplicity is mild, in contrast to the vigorously growing multiplicity seen by ALICE [32] for inclusive production. Our evaluation is largely parameter free and relies only on the choice of the parametrization for the dipole cross section (22).

We expect that suggested processes might be studied by the CMS (see their recent feasibility study in Ref. [20]), ALICE [32,102], and STAR collaborations.

ACKNOWLEDGMENTS

We thank our colleagues at UTFSM university for encouraging discussions. This research was partially supported by the project ANID PIA/APOYO, Project No. AFB180002(Chile) and Fondecyt (Chile) Grant No. 1180232. Also, we thank Yuri Ivanov for technical support of the USM HPC cluster, where some evaluations were performed.

APPENDIX A: EVALUATION OF THE DIPOLE AMPLITUDES

1. Single diffractive production

In this Appendix, for the sake of completeness, we explain the main technical steps and assumptions used for the derivation of the single diffractive cross section (2), (8). The general rules which allow us to express the cross sections of hard processes in terms of the color-singlet dipole cross section might be found in Refs. [51–59]. In the heavy quark mass limit, the strong coupling $\alpha_s(m_Q)$ is small, which allows us to consider the interaction of a heavy $\bar{Q}Q$ dipole with gluons perturbatively and discuss them similar to the treatment of the k_T-factorization approach. At the same time, we tacitly assume that each such gluon should be understood as a parton shower ("Pomeron").

In the high-energy eikonal picture, the interaction of the quarks and antiquark with a t-channel gluon are described by a factor $\pm igt^a\gamma(\boldsymbol{x}_\perp)$, where $\boldsymbol{x}_\perp$ is the transverse coordinate of the quark and the function $\gamma(\boldsymbol{x}_\perp)$ is related to a distribution of gluons in the target. The relation of this function with dipole cross-section $\sigma(x,\boldsymbol{r})$ might be found evaluating the diagrams shown in the Fig. 13, and has a form

$$\Delta\sigma(x,\boldsymbol{r}) \equiv \sigma(x,\infty) - \sigma(x,\boldsymbol{r}) = \frac{1}{8}\int d^2b|\gamma(x,\boldsymbol{b}-z\boldsymbol{r}) - \gamma(x,\boldsymbol{b}+\bar{z}\boldsymbol{r})|^2, \quad \text{(A1)}$$

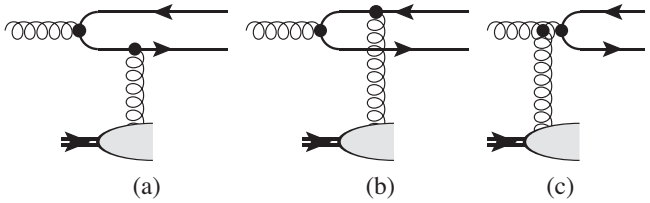

FIG. 13. The diagrams which contribute to the heavy meson production cross section in the leading-order perturbative QCD. The contribution of the last diagram (c) to the meson formation might be also viewed as gluon-gluon fusion $gg \to g$ with subsequent fragmentation $g \to \bar{Q}Q$. In CGC parametrization of the dipole cross section approach, each "gluon" is replaced with Reggeized gluon (BK Pomeron), which satisfies the Balitsky-Kovchegov equation and corresponds to a fanlike shower of soft particles.

where $\boldsymbol{r}$ is the transverse size of the dipole and z is the light-cone fraction of the dipole momentum carried by the quarks. The equation (A1) might be rewritten in the form

$$\frac{1}{8}\int d^2\boldsymbol{b}\gamma(x,\boldsymbol{b})\gamma(x,\boldsymbol{b}+\boldsymbol{r}) = \frac{1}{2}\sigma(x,\boldsymbol{r}) + \underbrace{\int d^2b|\gamma(x,\boldsymbol{b})|^2 - \frac{1}{2}\sigma(x,\infty)}_{=\text{const}}. \quad \text{(A2)}$$

For very small dipoles, the dipole cross section is related to the gluon uPDF as [122]

$$\sigma(x,\vec{\boldsymbol{r}}) = \frac{4\pi\alpha_s}{3}\int\frac{d^2k_\perp}{k_\perp^2}\mathcal{F}(x,k_\perp)(1-e^{ik\cdot r}) + \mathcal{O}\left(\frac{\Lambda_{\rm QCD}}{m_c}\right), \quad \text{(A3)}$$

so the functions $\gamma(x,\boldsymbol{r})$ might be also related to the unintegrated gluon densities. With the help of (A2), for many high-energy processes, it is possible to express the exclusive amplitude or inclusive cross section as a linear combination of the *color-singlet* dipole cross sections $\sigma(x,\boldsymbol{r})$ with different arguments. While in the deeply saturated regime we can no longer speak about individual gluons (or Pomerons), we expect that the relations between the dipole amplitudes and color-singlet cross sections should be valid even in this case.

For the case of single diffractive heavy quark pair production, the leading-order contribution is given by the diagrams shown in Fig. 14. As was explained at the beginning of this Appendix, in the heavy quark mass limit, the interactions of $\bar{Q}Q$ with gluons become perturbative, which implies that the t-channel Pomeron might be considered as a color-singlet pair of gluons. Taking into account all the diagrams shown in Fig. 14 and properties of the $SU(N_c)$ structure constants, we may express the amplitude of the single diffractive process as

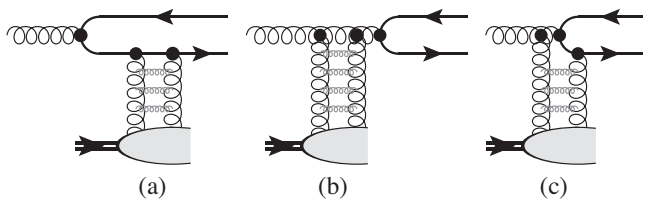

FIG. 14. The diagrams which contribute to the single diffractive heavy meson production in the leading order in perturbative QCD [$\mathcal{O}(\alpha_s)$ correction]. In diagrams (a) and (c), all possible attachments of the gluon to the quarks and antiquarks are implied. In QCD, the interaction of the color dipole with a Pomeron might be understood as a gluon ladder (BFKL Pomeron), and for this reason, its interaction with a dipole is described as with a pair of gluons in a color singlet state (see the text for explanation).

$$\mathcal{A}^{(3)}(x,\vec{\boldsymbol{r}}_Q,\vec{\boldsymbol{r}}_{\bar{Q}}) = \left[\frac{N_c}{4}\gamma_+^2(x,\vec{\boldsymbol{r}}_Q,\vec{\boldsymbol{r}}_{\bar{Q}}) + \left(\frac{N_c^2-4}{4N_c}+\frac{1}{6}\right)\gamma_-^2(x,\vec{\boldsymbol{r}}_Q,\vec{\boldsymbol{r}}_{\bar{Q}})\right]t_a \equiv a(x,\vec{\boldsymbol{r}}_Q,\vec{\boldsymbol{r}}_{\bar{Q}})t_a,$$

where

$$\gamma_+(x,\vec{\boldsymbol{r}}_1,\vec{\boldsymbol{r}}_2) = \gamma(x,\vec{\boldsymbol{r}}_1)+\gamma(x,\vec{\boldsymbol{r}}_2)-2\gamma\left(x,\frac{\vec{\boldsymbol{r}}_1+\vec{\boldsymbol{r}}_2}{2}\right),$$
$$\gamma_-(x,\vec{\boldsymbol{r}}_1,\vec{\boldsymbol{r}}_2) = \gamma(x,\vec{\boldsymbol{r}}_1)-\gamma(x,\vec{\boldsymbol{r}}_2),$$

a is the color index of the incident (projectile) gluon, and $\vec{\boldsymbol{r}}_Q$ and $\boldsymbol{r}_{\bar{Q}}$ are the coordinates of the quarks. For evaluation of the p_T dependent cross section, we need to project the coordinate space quark distribution onto the state with definite transverse momentum $\boldsymbol{p}_T$, so we have to evaluate the additional convolution approximately $\int d^2r_1 d^2r_2 e^{ip_T\cdot(r_1-r_2)}$, where $\vec{\boldsymbol{r}}_{1,2}$ are the coordinates of the quark in the amplitude and its conjugate, viz.,

$$\begin{aligned}|\mathcal{A}^{(3)}(\boldsymbol{p}_T)|^2 &= (1+\eta^2)\int d^2\boldsymbol{x}_{\bar{Q}}\int d^2\boldsymbol{x}_Q \times\int d^2\boldsymbol{y}_Q e^{i\boldsymbol{p}_T\cdot(\boldsymbol{x}_Q-\boldsymbol{y}_Q)}(\mathcal{A}^{(3)}(\vec{\boldsymbol{x}}_i))^*\mathcal{A}^{(3)}(\vec{\boldsymbol{y}}_i)|_{\vec{\boldsymbol{x}}_{\bar{Q}}=\vec{\boldsymbol{y}}_{\bar{Q}}}\\ &= \left(\frac{1+\eta^2}{2}\right)\int d^2\boldsymbol{x}_{\bar{Q}}\int d^2\boldsymbol{x}_Q \times\int d^2\boldsymbol{y}_Q e^{i\boldsymbol{p}_T\cdot(\boldsymbol{x}_Q-\boldsymbol{y}_Q)}a^*(x,\vec{\boldsymbol{x}}_Q,\vec{\boldsymbol{x}}_{\bar{Q}})a(x,\vec{\boldsymbol{y}}_Q,\vec{\boldsymbol{x}}_{\bar{Q}}).\end{aligned} \tag{A4}$$

As discussed earlier, at high energies, we may apply iteratively the relation (A1) and express the three-Pomeron dipole amplitude in terms of the color-singlet dipole cross sections, as given in (8). In the frame where the momentum of the primordial gluon is not zero, we should take into account an additional convolution with the momentum distribution of the incident ("primordial") gluons, as shown in (2) and as was demonstrated in Ref. [28].

2. Inclusive production

In Sec. III, we compared predictions for single diffractive production of heavy quarks with those of the inclusive production of the same mesons. For the sake of completeness, in this Appendix, we would like to mention briefly the main expressions used for evaluation of the cross sections for the latter case. A detailed discussion of inclusive production as well as comparison with experimental data might be found in Ref. [41]. The evaluation of the cross section follows the steps outlined in Appendix A 1. The leading-order contribution in the inclusive case is due to a standard fusion of two gluons (Pomerons). In the evaluation of the three-Pomeron contribution, we should take into account that there are two complementary mechanisms, shown schematically in Fig. 15. In what follows, we will refer to the contribution shown in the diagram (a) as genuine three-Pomeron corrections, whereas the contribution of the diagram (b) is the interference term. The two diagrams differ by number of cut Pomerons, and for this reason, they have a different multiplicity dependence. As we discussed in Ref. [41], both twist-3 corrections give sizeable contributions at small $p_T \lesssim 5$ GeV. For D mesons, the two corrections together contribute up to 40%–50% of the leading-order result, whereas for B mesons, these contributions are of order 10% even for $p_T \sim 0$, in agreement with the heavy mass limit.

Both the leading-order cross section and the higher twist correction might be written as

$$\begin{aligned}\frac{d\sigma_{pp\to\bar{Q}_iQ_i+X}(y,\sqrt{s})}{dyd^2p_T} &= \int d^2k_T x_1 g(x_1,\boldsymbol{p}_T-\boldsymbol{k}_T)\int_0^1 dz\int_0^1 dz' \times\int\frac{d^2r_1}{4\pi}\int\frac{d^2r_2}{4\pi}e^{i(r_1-r_2)\cdot\boldsymbol{k}_T}\Psi^\dagger_{\bar{Q}Q}(r_2,z,p_T) \times\Psi^\dagger_{\bar{Q}Q}(r_1,z,p_T)N_M(x_2(y);\vec{r}_1,\vec{r}_2)+(x_1\leftrightarrow x_2)\end{aligned} \tag{A5}$$

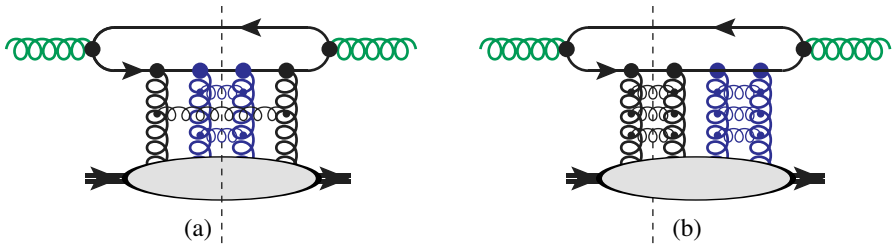

FIG. 15. The three-Pomeron contributions [diagram (a)] contribute at the same order in α_s as the interference of leading-order and next-to-next-to-leading-order diagrams [diagram (b)]. In both plots, the vertical dashed line is a unitary cut, the lower blob is a target (proton), and all possible connections of Pomerons (thick wavy lines) to the heavy Q, $\bar{Q}$ quark lines are implied. Note that in diagram (a) both Pomerons are cut, whereas in the case of the interference contribution, one of the Pomerons is uncut.

(see the Sec. II for notations and definitions). For the leading-order contribution, the amplitude N_M is given by [28,41]

$$N_M^{(2)}(x,\vec{r}_1,\vec{r}_2) = -\frac{1}{2}N(x,\vec{r}_1-\vec{r}_2) - \frac{1}{16}[N(x,\vec{r}_1)+N(x,\vec{r}_2)] - \frac{9}{8}N(x,\bar{z}(\vec{r}_1-\vec{r}_2)) + \frac{9}{16}[N(x,\bar{z}\vec{r}_1-\vec{r}_2) + N(x,\bar{z}\vec{r}_2-\vec{r}_1) + N(x,\bar{z}\vec{r}_1) + N(x,\bar{z}\vec{r}_2)]. \quad \text{(A6)}$$

Similarly, the three-Pomeron contribution shown in the diagram (a) of Fig. 15 may be rewritten as

$$N_M^{(3)}(x,z,\vec{r}_1,\vec{r}_2) \approx \frac{1}{8\sigma_{\rm eff}}\left[N_+^2(x,z,\vec{r}_1,\vec{r}_2)\left(\frac{3N_c^2}{8}\right) + N_-^2(x,\vec{r}_1,\vec{r}_2)\left(\frac{(43N_c^4-320N_c^2+720)}{72N_c^2}\right) + \frac{(N_c^2-4)}{2}N_+(x,z,\vec{r}_1,\vec{r}_2)N_-(x,\vec{r}_1,\vec{r}_2)\right], \quad \text{(A7)}$$

where

$$N_-(x,\vec{r}_1,\vec{r}_2) \equiv -\frac{1}{2}[N(x,\vec{r}_2-\vec{r}_1) - N(x,\vec{r}_1) - N(x,\vec{r}_2)] \quad \text{(A8)}$$

$$N_+(x,z,\vec{r}_1,\vec{r}_2) \equiv -\frac{1}{2}[N(x,\vec{r}_2-\vec{r}_1)+N(x,\vec{r}_1)+N(x,\vec{r}_2)] + N(x,\bar{z}\vec{r}_1-\vec{r}_2) + N(x,\bar{z}\vec{r}_1) + N(x,-\bar{z}\vec{r}_2+\vec{r}_1) + N(x,-\bar{z}\vec{r}_2) - 2N(x,\bar{z}(\vec{r}_1-\vec{r}_2)) \quad \text{(A9)}$$

and $\sigma_{\rm eff} \approx 20$ mb is a numerical parameter. Finally, for the interference term shown in Fig. 15(b), we may get in a similar way

$$N_M^{(\rm int)}(x,z,\vec{r}_1,\vec{r}_2) = -\frac{3}{16\sigma_{\rm eff}}\left[2N_+(x,z,\vec{r}_1,\vec{r}_2)\tilde{N}_+(x,z,\vec{r}_2)\left(\frac{3N_c^2}{8}\right) + -N_-(z,\vec{r}_1,\vec{r}_2)\tilde{N}_-(x,\vec{r}_2)\left(\frac{(43N_c^4-320N_c^2+720)}{72N_c^2}\right) + \frac{(N_c^2-4)}{2}(N_+(z,\vec{r}_1,\vec{r}_2)\tilde{N}_-(x,\vec{r}_2)+\tilde{N}_+(x,\vec{r}_2)N_-(z,\vec{r}_1,\vec{r}_2))\right]. \quad \text{(A10)}$$

APPENDIX B: FRAGMENTATION FUNCTIONS

For the sake of completeness, in this Appendix, we briefly summarize the fragmentation functions used in our evaluations. Since the fragmentation functions are essentially nonperturbative and cannot be evaluated from first principles, currently their parametrization is extracted from the phenomenological fits of e^+e^- annihilation data. For the B mesons, the dominant contribution comes from the fragmentation of b quarks, and for the fragmentation function of this process, we used the parametrization from Ref. [25]

$$D_{b\to B}(z,\mu_0) = Nz^\alpha(1-z)^\beta, \quad \text{(B1)}$$

where $N = 56.4$, $\alpha = 8.39$, and $\beta = 1.16$. The shape of parametrization (B1) is close to another widely used parametrization from [123]

$$D_{b\to B}(z,\mu_0) = \frac{N}{z(1-\frac{1}{z}-\frac{\epsilon}{1-z})^2}, \quad \text{(B2)}$$

$$\epsilon \approx 0.0126. \quad \text{(B3)}$$

The production of nonprompt charmonia which stem from decays of the B mesons might also be described using a fragmentation function, which is related to that of B mesons as [26]

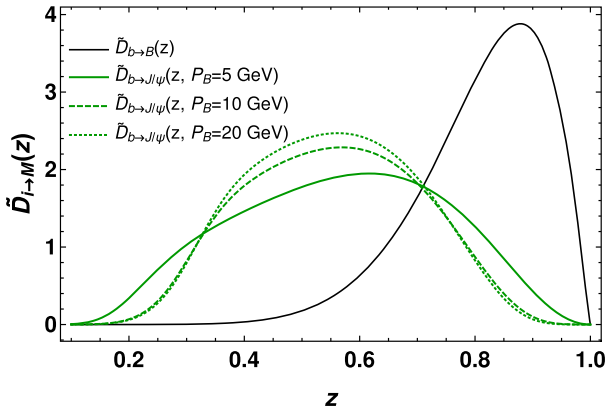

FIG. 16. The fragmentation function of B quarks and nonprompt J/ψ mesons. To facilitate comparison of the shapes, we normalized all the fragmentation functions to unity (so, we use the notation $\tilde{D}_{i\to M}$ instead of $D_{i\to M}$). The normalization coefficients for $b \to B$ and $b \to J/\psi$ cases differ by the branching fraction $Br_{B\to J/\psi} \approx 0.8\%$.

TABLE II. The values of parameters of D meson fragmentation function with parametrization (B4), as found in Ref. [124].

Meson	N_c	a_c	γ_c	N_b	a_b	γ_b
D^0	8.8×10^6	1.54	3.58	78.5	5.76	1.14
D^+	5.67×10^5	1.16	3.39	185	7.08	1.42

$$D_{b\to J/\psi}(z,\mu) = \int_z^1 dx D_{b\to B}\left(\frac{x}{z},\mu^2\right) \times \frac{1}{\Gamma_B}\frac{d\Gamma}{dz}(z,P_B),$$

where $\Gamma_B \equiv 1/\tau_B$ is the total decay width of the B meson and the function $d\Gamma(z,P_B)/dz$ was evaluated in detail in Ref. [26]. In Fig. 16, we compare the fragmentation functions $D_{b\to B}$ and $D_{b\to J/\psi}$. These two functions differ by the branching fraction $Br_{B\to J/\psi} \approx 0.8\%$, and for this reason, in order to facilitate comparison, we plotted the fragmentation functions normalized to unity, $\tilde{D}(z) = D(z)/\int_0^1 dz D(z)$. As we can see, the distribution $D_{b\to J/\psi}$ is significantly wider than $D_{b\to B}$ and has a peak near smaller values of $z \approx 0.5$.

The D mesons might be produced either from fragmentation of c quarks (prompt mechanism) or from b quarks (nonprompt mechanism). The fragmentation functions for both cases are available from Ref. [124],

$$D_{i\to D}(z,\mu_0) = N_i z^{-(1+\gamma_i^2)}(1-z)^a \exp(-\gamma_i^2/z), \quad i = b,c \tag{B4}$$

with parameters given in Table II. Though the parameters for D^+ and D^0 in the table differ significantly, their fragmentation functions have very similar shapes and differ only by a factor of 2 in normalization.

APPENDIX C: PARAMETRIZATION FOR THE MATRIX Ω_{ik}

In this Appendix, we briefly summarize the parametrization of the soft Pomeron scattering amplitude Ω_{ik} used in Sec. II B. In the two-channel model, it is assumed that in addition to proton there is another diffractive state X, which might be produced instead of proton in inelastic processes (e.g., single diffractive and double diffractive). The matrix Ω_{ik} is thus a 2×2 matrix in the subspace which includes a proton and the diffractive state X.

For our evaluations, we used a parametrization from Ref. [46], which has the form

$$\Omega_{ik}(b,s) = \int \frac{d^2q}{4\pi^2} e^{iq\cdot b}\tilde{\Omega}_{ik}(t=-q^2,s) \tag{C1}$$

$$\tilde{\Omega}_{ik}(t,s) = v_i F_i(t) F_k(t)\left(\frac{s}{s_0}\right)^{\alpha_{\rm IP}-1}, \tag{C2}$$

$$F_i(t) = \exp\left(b_i(c_i^{d_i} - (c_i - t)^{d_i})\right), \tag{C3}$$

$$s_0 \approx 1\ \text{GeV}^2, \qquad v_{1,2} = \sqrt{\sigma_0}(1\pm\lambda), \tag{C4}$$

$$\sigma_0 \approx 23\ \text{mb}, \qquad \lambda \approx 0.56, \tag{C5}$$

$$b_1 \approx 10\ \text{GeV}^{-2}, \qquad b_2 \approx 4.9\ \text{GeV}^{-2}, \tag{C6}$$

$$c_1 \approx 0.233\ \text{GeV}^2, \qquad c_2 \approx 0.52\ \text{GeV}^2, \tag{C7}$$

$$d_1 \approx 0.462, \qquad d_2 \approx 0.47, \tag{C8}$$

$$\alpha_{\rm IP}(t) \approx 1.13 + 0.052t \tag{C9}$$

and has been fitted using recent LHC data on elastic, single diffractive, and double diffractive scattering.

[1] B. Abelev *et al.* (ALICE Collaboration), Eur. Phys. J. C **73**, 2456 (2013).
[2] A. Cisek, W. Schäfer, and A. Szczurek, Phys. Lett. B **769**, 176 (2017).
[3] M. V. T. Machado, Braz. J. Phys. **38**, 416 (2008).
[4] M. V. T. Machado, Eur. Phys. J. C **54**, 443 (2008).
[5] F. Yuan and K. T. Chao, Phys. Rev. D **57**, 5658 (1998).
[6] F. Yuan, J. S. Xu, H. A. Peng, and K. T. Chao, Phys. Rev. D **58**, 114016 (1998).
[7] H. Mantysaari, N. Mueller, and B. Schenke, Phys. Rev. D **99**, 074004 (2019).
[8] R. S. Pasechnik, B. Z. Kopeliovich, and I. K. Potashnikova, Phys. Rev. D **86**, 114039 (2012).
[9] R. Pasechnik, B. Z. Kopeliovich, and I. K. Potashnikova, Phys. Rev. D **92**, 094014 (2015).
[10] B. Z. Kopeliovich, I. K. Potashnikova, I. Schmidt, and A. V. Tarasov, Phys. Rev. D **76**, 034019 (2007).
[11] M. Łuszczak, R. Maciuła, and A. Szczurek, Phys. Rev. D **91**, 054024 (2015).
[12] M. Luszczak, R. Maciula, A. Szczurek, and M. Trzebinski, J. High Energy Phys. 02 (2017) 089.
[13] C. Brenner Mariotto, V. P. Goncalves, and R. P. da Silva, arXiv:1806.04029.
[14] B. Z. Kopeliovich, I. K. Potashnikova, I. Schmidt, and A. V. Tarasov, Phys. Rev. D **74**, 114024 (2006).
[15] T. Affolder *et al.* (CDF Collaboration), Phys. Rev. Lett. **87**, 241802 (2001).

[16] T. Affolder *et al.* (CDF Collaboration), Phys. Rev. Lett. **84**, 232 (2000).
[17] T. Aaltonen *et al.* (CDF Collaboration), Phys. Rev. D **86**, 032009 (2012).
[18] T. Aaltonen *et al.* (CDF Collaboration), Phys. Rev. D **82**, 112004 (2010).
[19] D. Acosta *et al.* (CDF Collaboration), Phys. Rev. Lett. **88**, 151802 (2002).
[20] CMS Collaboration, CMS-TOTEM feasibility studies for single diffractive Z, W, Jpsi and central exclusive dijet production in pp collisions at 13 TeV, CERN Report No. CMS-PAS-FSQ-14-001, 2014.
[21] J. G. Korner and G. Thompson, Phys. Lett. B **264**, 185 (1991).
[22] M. Neubert, Phys. Rep. **245**, 259 (1994).
[23] G. T. Bodwin, E. Braaten, and G. P. Lepage, Phys. Rev. D **51**, 1125 (1995); **55**, 5853(E) (1997).
[24] F. Maltoni, M. L. Mangano, and A. Petrelli, Nucl. Phys. **B519**, 361 (1998).
[25] J. Binnewies, B. A. Kniehl, and G. Kramer, Phys. Rev. D **58**, 034016 (1998).
[26] B. A. Kniehl and G. Kramer, Phys. Rev. D **60**, 014006 (1999).
[27] Y. Q. Ma, P. Tribedy, R. Venugopalan, and K. Watanabe, Phys. Rev. D **98**, 074025 (2018).
[28] V. P. Goncalves, B. Kopeliovich, J. Nemchik, R. Pasechnik, and I. Potashnikova, Phys. Rev. D **96**, 014010 (2017).
[29] N. Brambilla, A. Vairo, and E. Mereghetti, Phys. Rev. D **79**, 074002 (2009); **83**, 079904(E) (2011).
[30] Y. Feng, J. P. Lansberg, and J. X. Wang, Eur. Phys. J. C **75**, 313 (2015).
[31] N. Brambilla *et al.*, Eur. Phys. J. C **71**, 1534 (2011).
[32] J. Adam *et al.* (ALICE Collaboration), J. High Energy Phys. 09 (2015) 148.
[33] B. Trzeciak (STAR Collaboration), J. Phys. Conf. Ser. **668**, 012093 (2016).
[34] R. Ma (STAR Collaboration), Nucl. Part. Phys. Proc. **276–278**, 261 (2016).
[35] D. Thakur (ALICE Collaboration), arXiv:1811.01535.
[36] A. Khatun (ALICE Collaboration), arXiv:1906.09877.
[37] B. Abelev *et al.* (ALICE Collaboration), Phys. Lett. B **712**, 165 (2012).
[38] L. Motyka and M. Sadzikowski, Eur. Phys. J. C **75**, 213 (2015).
[39] E. Levin and M. Siddikov, Eur. Phys. J. C **79**, 376 (2019).
[40] E. Levin, I. Schmidt, and M. Siddikov, Eur. Phys. J. C **80**, 560 (2020).
[41] I. Schmidt and M. Siddikov, Phys. Rev. D **101**, 094020 (2020).
[42] ATLAS Collaboration, arXiv:1307.7292.
[43] G. Apollinari *et al.*, *High-Luminosity Large Hadron Collider (HL-LHC): Technical Design Report V. 0.1*, CERN Yellow Reports: Monographs (CERN, Geneva, 2017).
[44] P. La Rocca and F Riggi, J. Phys. Conf. Ser. **515**, 012012 (2014).
[45] A. D. Martin, V. A. Khoze, and M. G. Ryskin, Rapidity gap survival probability and total cross sections, https://doi.org/10.3204/DESY-PROC-2009-02/15 (2008).
[46] V. Khoze, A. Martin, and M. Ryskin, Phys. Lett. B **784**, 192 (2018).
[47] M. Ryskin, A. Martin, and V. Khoze, Eur. Phys. J. C **60**, 249 (2009).
[48] V. Khoze, A. D. Martin, and M. G. Ryskin, Eur. Phys. J. C **18**, 167 (2000).
[49] V. Khoze, A. Martin, and M. Ryskin, J. Phys. G **45**, 053002 (2018).
[50] G. Ingelman and P. E. Schlein, Phys. Lett. **152B**, 256 (1985).
[51] L. V. Gribov, E. M. Levin, and M. G. Ryskin, Phys. Rep. **100**, 1 (1983).
[52] L. D. McLerran and R. Venugopalan, Phys. Rev. D **49**, 2233 (1994).
[53] L. D. McLerran and R. Venugopalan, Phys. Rev. D **49**, 3352 (1994).
[54] L. D. McLerran and R. Venugopalan, Phys. Rev. D **50**, 2225 (1994).
[55] A. H. Mueller and J. Qiu, Nucl. Phys. **B268**, 427 (1986).
[56] L. McLerran and R. Venugopalan, Phys. Rev. D **49**, 3352 (1994); Phys. Rev. D **50**, 2225 (1994); Phys. Rev. D **59**, 094002 (1999).
[57] K. J. Golec-Biernat and M. Wusthoff, Phys. Rev. D **60**, 114023 (1999).
[58] B. Z. Kopeliovich and A. V. Tarasov, Nucl. Phys. **A710**, 180 (2002).
[59] B. Kopeliovich, A. Tarasov, and J. Hufner, Nucl. Phys. **A696**, 669 (2001).
[60] N. N. Nikolaev and B. G. Zakharov, J. Exp. Theor. Phys. **78**, 598 (1994), http://www.jetp.ac.ru/cgi-bin/e/index/e/78/5/p598?a=list.
[61] Y. V. Kovchegov, Phys. Rev. D **60**, 034008 (1999).
[62] Y. V. Kovchegov and H. Weigert, Nucl. Phys. **A784**, 188 (2007).
[63] I. Balitsky and G. A. Chirilli, Phys. Rev. D **77**, 014019 (2008).
[64] Y. V. Kovchegov and E. Levin, Cambridge Monogr. Part. Phys., Nucl. Phys., Cosmol. **33**, 1 (2012).
[65] I. Balitsky, Phys. Lett. B **518**, 235 (2001).
[66] F. Cougoulic and Y. V. Kovchegov, Phys. Rev. D **100**, 114020 (2019).
[67] C. A. Aidala *et al.*, arXiv:2002.12333.
[68] Y. Q. Ma and R. Venugopalan, Phys. Rev. Lett. **113**, 192301 (2014).
[69] Y. V. Kovchegov and E. Levin, *Quantum Chromodynamics at High Energy* (Cambridge University Press, Cambridge, England, 2012), Vol. 33.
[70] D. Kharzeev and M. Nardi, Phys. Lett. B **507**, 121 (2001); D. Kharzeev and E. Levin, Phys. Lett. B **523**, 79 (2001); D. Kharzeev, E. Levin, and M. Nardi, Phys. Rev. C **71**, 054903 (2005); J. Phys. G **35**, 054001 (2008).
[71] A. Dumitru, D. E. Kharzeev, E. M. Levin, and Y. Nara, Phys. Rev. C **85**, 044920 (2012).
[72] D. Kharzeev and M. Nardi, Phys. Lett. B **507**, 121 (2001).
[73] Y. V. Kovchegov, Nucl. Phys. **A692**, 557 (2001).
[74] E. Levin and A. H. Rezaeian, Phys. Rev. D **82**, 014022 (2010).
[75] T. Lappi, Eur. Phys. J. C **71**, 1699 (2011).
[76] A. H. Rezaeian, M. Siddikov, M. Van de Klundert, and R. Venugopalan, Phys. Rev. D **87**, 034002 (2013).
[77] H. G. Dosch, T. Gousset, G. Kulzinger, and H. J. Pirner, Phys. Rev. D **55**, 2602 (1997).

[78] H. Kowalski and D. Teaney, Phys. Rev. D **68**, 114005 (2003).
[79] H. Kowalski, L. Motyka, and G. Watt, Phys. Rev. D **74**, 074016 (2006).
[80] A. H. Rezaeian and I. Schmidt, Phys. Rev. D **88**, 074016 (2013).
[81] R. S. Thorne, AIP Conf. Proc. **792**, 324 (2005).
[82] M. A. Kimber, A. D. Martin, and M. G. Ryskin, Phys. Rev. D **63**, 114027 (2001).
[83] M. L. Good and W. D. Walker, Phys. Rev. **120**, 1857 (1960); E. L. Feinberg and I. Ya. Pomeranchuk, Dokl. Akad. Nauk SSSR **93**, 439 (1953); Suppl. Nuovo Cimento **III**, 652 (1956).
[84] E. Gotsman, H. Kowalski, E. Levin, U. Maor, and A. Prygarin, Eur. Phys. J. C **47**, 655 (2006).
[85] E. Gotsman, E. Levin, U. Maor, E. Naftali, and A. Prygarin, arXiv:hep-ph/0511060.
[86] M. Ryskin, A. Martin, V. Khoze, and A. Shuvaev, J. Phys. G **36**, 093001 (2009).
[87] A. Bialas and R. B. Peschanski, Phys. Lett. B **378**, 302 (1996).
[88] E. Gotsman, E. Levin, and U. Maor, Phys. Lett. B **452**, 387 (1999).
[89] V. A. Khoze, A. D. Martin, and M. G. Ryskin, Int. J. Mod. Phys. A **30**, 1542004 (2015).
[90] V. A. Khoze, A. D. Martin, and M. G. Ryskin, Eur. Phys. J. C **18**, 167 (2000).
[91] B. Alver *et al.* (PHOBOS Collaboration), Phys. Rev. C **75**, 054913 (2007).
[92] K. Eggert *et al.* (ISR Collaboration), Nucl. Phys. **B86**, 201 (1975).
[93] V. Khachatryan *et al.* (CMS Collaboration), J. High Energy Phys. 09 (2010) 091.
[94] S. Acharya *et al.* (ALICE Collaboration), Eur. Phys. J. C **77**, 550 (2017).
[95] M. Mangano, CERN Yellow Reports: Monographs (CERN, Geneva, 2017), Vol. 3.
[96] V. Khachatryan *et al.* (CMS Collaboration), Phys. Lett. B **771**, 435 (2017).
[97] G. Aad *et al.* (ATLAS Collaboration), J. High Energy Phys. 10 (2013) 042.
[98] S. Chatrchyan *et al.* (CMS Collaboration), J. High Energy Phys. 02 (2012) 011.
[99] Y. L. Dokshitzer, V. A. Khoze, and S. I. Troian, J. Phys. G **17**, 1585 (1991).
[100] V. A. Khoze, W. Ochs, and J. Wosiek, Analytical QCD and multiparticle production, *At The Frontier of Particle Physics*, edited by M. Shifman (World Scientific, Singapore, 2001), pp. 1101–1194.
[101] V. A. Khoze and W. Ochs, Int. J. Mod. Phys. A **12**, 2949 (1997).
[102] B. Abelev *et al.* (ALICE Collaboration), Phys. Lett. B **712**, 165 (2012).
[103] D. Thakur (ALICE Collaboration), Springer Proc. Phys. **234**, 217 (2019).
[104] E. V. Shuryak, Sov. J. Nucl. Phys. **28**, 408 (1978) [Phys. Lett. **78B**, 150 (1978)].
[105] E. V. Shuryak, Phys. Rep. **61**, 71 (1980).
[106] P. Braun-Munzinger and J. Stachel, Nature (London) **448**, 302 (2007).
[107] K. Fukushima and F. Gelis, Nucl. Phys. **A874**, 108 (2012).
[108] J. D. Bjorken, Phys. Rev. D **27**, 140 (1983).
[109] I. Schmidt, M. Siddikov, and M. Musakhanov, Phys. Rev. C **98**, 025207 (2018).
[110] J. C. Collins and M. J. Perry, Phys. Rev. Lett. **34**, 1353 (1975).
[111] Y. Li and K. Tuchin, Phys. Rev. D **77**, 114012 (2008).
[112] K. Tuchin, Phys. Rev. C **79**, 055206 (2009).
[113] R. J. Glauber, Phys. Rev. **100**, 242 (1955).
[114] R. J. Glauber and G. Matthiae, Nucl. Phys. **B21**, 135 (1970).
[115] V. N. Gribov, Sov. Phys. JETP **29**, 483 (1969), http://www.jetp.ac.ru/cgi-bin/e/index/e/29/3/p483?a=list.
[116] J. L. Albacete *et al.*, Nucl. Phys. **A972**, 18 (2018).
[117] J. L. Albacete *et al.*, Int. J. Mod. Phys. E **25**, 1630005 (2016).
[118] K. J. Eskola, H. Paukkunen, and C. A. Salgado, J. High Energy Phys. 04 (2009) 065.
[119] B. Z. Kopeliovich, I. Schmidt, and M. Siddikov, Phys. Rev. C **95**, 065203 (2017).
[120] J. L. Albacete, N. Armesto, J. G. Milhano, C. A. Salgado, and U. A. Wiedemann, Phys. Rev. D **71**, 014003 (2005).
[121] J. L. Albacete, N. Armesto, J. G. Milhano, C. A. Salgado, and U. A. Wiedemann, Eur. Phys. J. C **43**, 353 (2005).
[122] In the literature, definitions of the unintegrated PDF $\mathcal{F}(x, k_\perp)$ might differ by a factor $k_\perp^2$.
[123] C. Peterson, D. Schlatter, I. Schmitt, and P. M. Zerwas, Phys. Rev. D **27**, 105 (1983).
[124] T. Kneesch, B. A. Kniehl, G. Kramer, and I. Schienbein, Nucl. Phys. **B799**, 34 (2008).